AN ANALYSIS OF THE REACTIVITY TEMPERATURE COEFFICIENT OF THE KANSAS STATE UNIVERSITY TRIGA MARK II NUCLEAR REACTOR

by 1264

GENE P. RATHBUN

B.S., Kansas State University, 1967

A MASTER'S THESIS

submitted in partial fulfillment of the

requirements for the degree

MASTER OF SCIENCE

Department of Nuclear Engineering

KANSAS STATE UNIVERSITY
Manhattan, Kansas

1969

Approved by:

M. John Robinson
Major Professor

CONTENTS

1.0 INTRODUCTION 1

2.0 REACTOR DESCRIPTION 5

3.0 THEORY OF THE TEMPERATURE COEFFICIENT 11

3.1 Definitions 11

3.2 Temperature Coefficients of the Parameters. 13

3.2.1 Reactivity 13

3.2.2 Resonance Escape Probability 14

3.2.3 Fast Fission Factor 16

3.2.4 The ηf Product 16

3.2.5 Thermal Nonleakage Probability . . . 26

3.2.6 Fast Nonleakage Probability 28

3.3 Results and Discussion 29

4.0 EXPERIMENTAL DETERMINATION OF THE TEMPERATURE COEFFICIENT 34

4.1 Experiment Design 34

4.1.1 Reactor Licensing 34

4.1.2 Insulated Instrumented Element . . . 35

4.2 Reactor System Initilization 38

4.2.1 Approach to Critical 38

4.2.2 Power Calibration 38

4.2.3 Control Rod Calibration 39

4.3 Experimental Equipment and Procedure . . . 39

4.3.1 Steady State Method 39

4.3.2 Transient Method 42

4.4 Results and Discussion 46

ILLEGIBLE DOCUMENT

THE FOLLOWING DOCUMENT(S) IS OF POOR LEGIBILITY IN THE ORIGINAL

THIS IS THE BEST COPY AVAILABLE

THIS BOOK CONTAINS NUMEROUS PAGES WITH DIAGRAMS THAT ARE CROOKED COMPARED TO THE REST OF THE INFORMATION ON THE PAGE.

THIS IS AS RECEIVED FROM CUSTOMER.

5.0 SUGGESTIONS FOR FURTHER STUDY 62

6.0 ACKNOWLEDGEMENTS 63

LITERATURE CITED 64

APPENDICES

APPENDIX A: Temperature Analysis of TRIGA Mark II Insulated Fuel Element. 68

APPENDIX B: ZIRK, A Scattering Kernel Code for Zirconium Hydride . . 77

APPENDIX C: GROUPS, A Program to Homogenize the TRIGA Cell . . . 83

APPENDIX D: SPECTRUM, A Code to Calculate the Flux Spectrum in the TRIGA Cell 89

LIST OF FIGURES

1. Elevation view of TRIGA Mark II 6
2. The upper and lower grid plates of the TRIGA . . 7
3. Exterior view of a TRIGA fuel element 8
4. Loading diagram 9
5. Fuel rod unit cell 19
6. Resonance escape probability as a function of temperature as calculated by RABBLE for the KSU TRIGA Mark II 30
7. The temperature dependence of the ηf product of the Kansas State University TRIGA Mark II Nuclear Reactor 32
8. The total temperature coefficient curve showing the contributions from all the parameters of k_{eff} 33
9. TRIGA instrumented fuel element 36
10. The insulated instrumented fuel element as it was used in the experimentation 37
11. Shim rod calibration curve 40
12. Reg rod calibration curve 41
13. Ideal temperature and power traces 43
14. Instrumentation used to measure the power 44
15. Instrumentation diagram of the equipment used to measure the transient temperature and power data. 45
16. Temperature and power traces of a typical transient run 48
17. Temperature of the insulated element plotted versus the worth of the shim rod remaining in the core following the power drop for the first four runs with the insulated element in the central thimble position 50

18. The worth of the shim rod remaining in the core plotted versus the temperature of the bare element following the power drop for the first four runs with the bare element in the central thimble position 51

19. The change in the worth from criticality at 90 kW of the control rods plotted versus the average B-ring temperatures of the twenty runs for both the bare and insulated cases 52

20. The effect of delayed neutrons, temperature, and control rod movement on reactivity when the insulated element was in the central thimble position 55

21. The effect of delayed neutrons, temperature, and control rod movement on reactivity when the bare element was in the central thimble position 56

22. Average core temperature versus power curves for the bare and insulated central thimble element cases. The measured B-ring temperature versus power curve is used as the standard for comparing the bare and insulated data 58

A.1. Temperature versus power plot for KSU TRIGA Mark II Reactor showing the centerline temperature predicted for an insulated fuel element in the central thimble position 74

A.2. Temperature versus radius plot for a KSU TRIGA Mark II Reactor fuel element at 100 kW . . . 76

B.1. A plot showing the effect of temperature on the scattering cross section of hydrogen in zirconium hydride 79

D.1. Flux spectra in the TRIGA core at temperatures of 293°K and 773°K 91

LIST OF TABLES

I. Steady state differential control rod worths . . 46

A.I. Temperature analysis of insulated fuel element in central thimble of TRIGA Mark II Reactor . . 75

NOMENCLATURE

A_{el}	mass number of element, el
B^2	geometric bucking of the core (cm^{-2})
D	diffusion coefficient (cm)
D_m	diffusion coefficient in material m
D_e	equivalent diameter of the channel of flow (ft)
E	neutron energy (eV)
E_o	initial neutron energy
f	thermal utilization
f_m	Moody's friction factor
g	gravitational accceleration (ft/sec^2)
g_c	conversion factor (32.174 lbm ft/lbf sec^2)
H	core height (ft)
h	heat transfer coefficient (BTU/hr ft^2 ^oF)
k_c	thermal conductivity of the clad (BTU/hr ft ^oF)
k_f	thermal conductivity of the fuel
k_w	thermal conductivity of water
k_{eff}	effective multiplication constant
L_i	diffusion length of material i (cm)
N	nuclear density (nuclei/cm^3)
N_{el}	nuclear density of element, el
$N_{H_{ZrH}}$	nuclear density of hydrogen in zirconium hydride
$N_{H_{H_2O}}$	nuclear density of hydrogen in water
$N(v)$	velocity dependent neutron density (neutrons/cm^3)
N_i	neutron density for group i
$N_i^{(k)}$	neutron density for group i after the kth iteration

Nu	Nusselt number
n	number of nuclei
p	resonance escape probability
P	nonleakage probability
P_{th}	thermal nonleakage probability
P_f	fast nonleakage probability
P_c	collision probability in a cylinder
P_{ij}	scattering kernel from group i to group j
Pr	Prandtl number
ΔP_f	friction pressure drop (lbf/ft^2)
ΔP_h	hydrostatic pressure drop
Q_i	slowing down power for region i
q'''	heat generation rate ($BTU/hr\ ft^3$)
R_{cf}	thermal conductance between the fuel and cladding ($BTU/hr\ ft^2\ ^oF$)
Re	Reynolds' number
R_j	radius of region i (cm)
r	a characteristic dimension of the system (cm)
r'	prompt neutron lifetime (sec)
S(v)	slowing down source of neutrons at velocity v ($neutrons/cm^3$ sec)
S_j	slowing down source of neutrons for group j
T_{max}	centerline fuel temperature (^oC)
T_{surf}	fuel surface temperature
T_f	bulk fluid temperature
T	temperature (^oC or ^oK)
t	time (sec)

t_2	thickness of the clad (cm)
$t(E)$	Fermi age at energy E (cm^2)
t_{th}	Fermi age at thermal energy
$\alpha_T(X)$	temperature coefficient of property X ($\not{\phi}/^oC$)
β	coefficient of volume expansion ($^oC^{-1}$)
β_i	coefficient of volume expansion for material i
β'	one group delay fraction
δ_{ij}	dirac delta function
ϵ	fast fission factor
η	average number of fission neutrons emitted per thermal neutron absorbed in the fuel
θ	the angle of neutron scattering
λ	one group decay constant (sec^{-1})
λ_3	extrapolation length for a black cylinder (cm)
μ	water viscosity (lbm/ft hr)
$\bar{\mu}$	average cosine of the scattering angle in the laboratory system
ξ_i	average logarithmic energy decrement per collision for element i
ρ	reactivity (dollars)
$\bar{\rho}$	water density (lbm/ft^3)
Σ_a	absorption cross section (cm^{-1})
Σ_f	fission cross section
Σ_s	scattering cross section
Σ_t	total cross section
Σ_{a_i}	absorption cross section for element or group or region i
Σ_{s_i}	scattering cross section for element or group or region i

Σ_{t_i}	total cross section for element or group or region i
$\Sigma^*_{s_i}$	scattering cross section for region i corrected for anisotropy
$\Sigma_{a,core}$	homogenized absorption cross section for the core
$\Sigma_{f,core}$	homogenized fission cross section for the core
$\Sigma_{s,core}$	homogenized scattering cross section for the core
$\Sigma_{s,el}$	scattering cross section for element, el
$\Sigma_{s,clad}$	scattering cross section of the clad
$\Sigma_{s,o}$	scattering cross section of oxygen
$\Sigma_t(v)$	total cross section at velocity v
$\Sigma_s(v' \rightarrow v)$	scattering kernel for scattering from velocity v' into velocity v
$\Sigma_s(i \rightarrow j)$	scattering kernel for scattering from group i to group j
σ_b	bound proton microscopic cross section (barns)
σ_f	effective fission cross section of the fuel
$\sigma_{i,el}$	microscopic cross section of type i for element, el
$\sigma_s(E_o, E, \theta)$	scattering kernel for neutrons of initial energy E_o scattering into energy E at angle θ
$\sigma_s(E_o, E)$	scattering kernel for neutrons of initial energy E_o scattering into energy E
$\sigma_s(E_o)$	scattering cross section for neutrons of initial energy E_o
$\sigma_s(i \rightarrow j)$	scattering cross section kernel for neutrons in group i scattering to group j
$\phi(t)$	neutron flux at time t (neutrons/cm^2 sec)
ϕ_i	neutron flux for group or region i
ϕ	thermal neutron flux

1.0 INTRODUCTION

A problem of considerable importance in the control of nuclear reactors is the design and evaluation of the temperature coefficient of the reactor system. The temperature coefficient is defined as the change in the multiplication constant of the system due to a change in the operating temperature of the reactor. Such variations may be localized, e.g., due to nonuniformity of coolant flow at particular points in the reactor, or they may effect the reactor as a whole such as the variations caused by an increase in the power level or coolant inlet temperature of the reactor.

The temperature coefficient is a measure of the stability of the reactor. If the coefficient is positive then an increase in temperature will cause the multiplication constant to increase, which would increase the energy production rate of the reactor thus resulting in a further temperature increase. Such a system is highly unstable and would require highly sensitive monitoring by the control systems to maintain steady-state conditions. For reactors with negative temperature coefficients, a temperature increase would cause the multiplication constant and power to decrease so that the temperature tends to decrease to its original value. Reactors having negative temperature coefficients are therefore stable with respect to temperature changes.

Special moderator materials are often used in order to insure the desired temperature coefficient. In zirconium

hydride, because the motion of the hydrogen atom is severly restricted by the chemical bonds which essentially tie it to an infinitely heavy crystal matrix, the motion can be approximated by the Einstein oscillator model (2, 3) with a suitably chosen frequency. The basic process involved when ZrH_n increases in temperature is a speeding up of the neutrons due to collisions whereby they gain an amount of energy from the increased number of oscillators in the first excited state. Because the neutrons are speeded up, there is a decrease in the fission probability and a consequent loss of reactivity. This effect is so efficient that ZrH_n moderated reactors are able to be pulsed with large amounts of excess reactivity with reasonable assurance that the pulse will be immediately compensated for without dependence on electrical or mechanical controls by the large negative temperature coefficient of this type of reactor.

The temperature coefficient of a reactor is a function of many other phenomena besides the moderator effect described above. Another effect that contributes to the temperature coefficient, is the Doppler broadening of the cross section resonance peaks with increasing temperature due to the increased random motion of the reacting nuclei.

The fuel-moderator elements of the Kansas State University TRIGA Mark II reactor are made of an alloy of uranium-zirconium hydride containing 8 weight per cent uranium enriched to 20 per cent in U-235 (1). Thus, because the moderator effect of the zirconium and the broadening of the cross section resonances in

the uranium contribute to the negative temperature coefficient dependence of the TRIGA, it is a very stable reactor.

The original goal of this paper was to determine the Doppler coefficient of the Kansas State University TRIGA Mark II reactor. It has been shown (8, 9, 12, 13) that the Doppler coefficient for fast reactors can be experimentally found by heating small samples of fuel in the center of the reactor core. Much of the work that has been done has involved oscillating samples of various temperatures in and out of low power fast critical assemblies (10, 14, 15). Doppler effects obtained by measuring the reactivity changes from heating samples are somewhat subject to masking effects due to simple thermal expansion. In order to counteract this masking, experiments have been performed (10, 14, 15) where special fuel elements were designed that allowed the fuel to expand against springs. Measurements of reactivity data were taken with the heated special element in the core and also with a heated regular element in the core. Then the Doppler coefficient could be found by differencing the constrained and unconstrained reactivity changes.

Since fabrication of such a spring - loaded element would have been too expensive and since oscillation of an element in and out of the TRIGA's core would have been impossible due to license limitations, the experimental portion of this thesis was designed to measure the total temperature coefficient. This coefficient includes expansion, moderator effects, and Doppler

effects. The temperature dependence of the parameters in the expression which describes the effective multiplication constant was developed so that a theoritical value of the temperature coefficient could be compared with the experimental value.

2.0 REACTOR DESCRIPTION

The TRIGA reactor core is located near the bottom of a pool, under nearly 16 feet of water which acts as coolant, moderator, and radiation shield. The core is cooled by natural convection of the water. The core is surrounded and supported by a one foot thick graphite reflector. Figure 1 shows a cut-away view of the core and reflector at the bottom of the reactor pool.

The fuel-moderator and graphite dummy elements are positioned in the core by upper and lower grid plates which are bracketed to the reflector. The upper grid plate is shown in Fig. 2.

The TRIGA fuel-moderator elements are a homogeneous alloy of uranium-zirconium hydride containing 8 weight per cent uranium enriched to 20 per cent in U-235. The fueled portion of each element is 1.42 inches in diameter by 14 inches in length. The elements are clad with 0.030 inch thick aluminum. Four inch sections of graphite in the fuel can above and below the fuel region serve as top and bottom reflectors. Each fuel element contains approximately 37 grams of U-235. A fuel element is shown in Fig. 3.

The loading diagram for normal operation of the reactor is given in Fig. 4. The elements form five concentric rings around the center position (the central thimble). These five rings are designated B, C, D, E and F, respectively from inside to outside.

The reactor is controlled by three boron carbide control

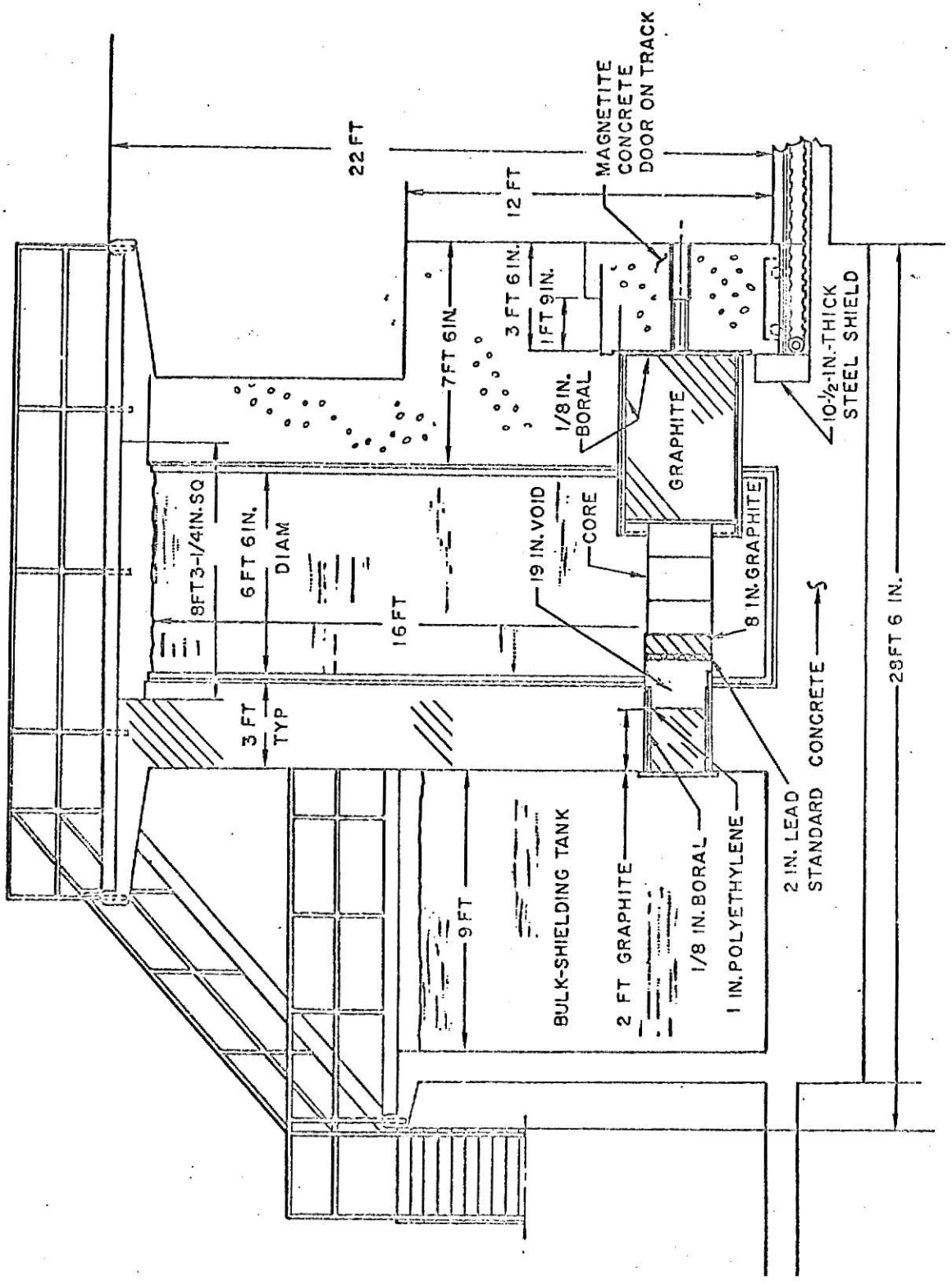

Fig. 1. Elevation view of TRIGA Mark II

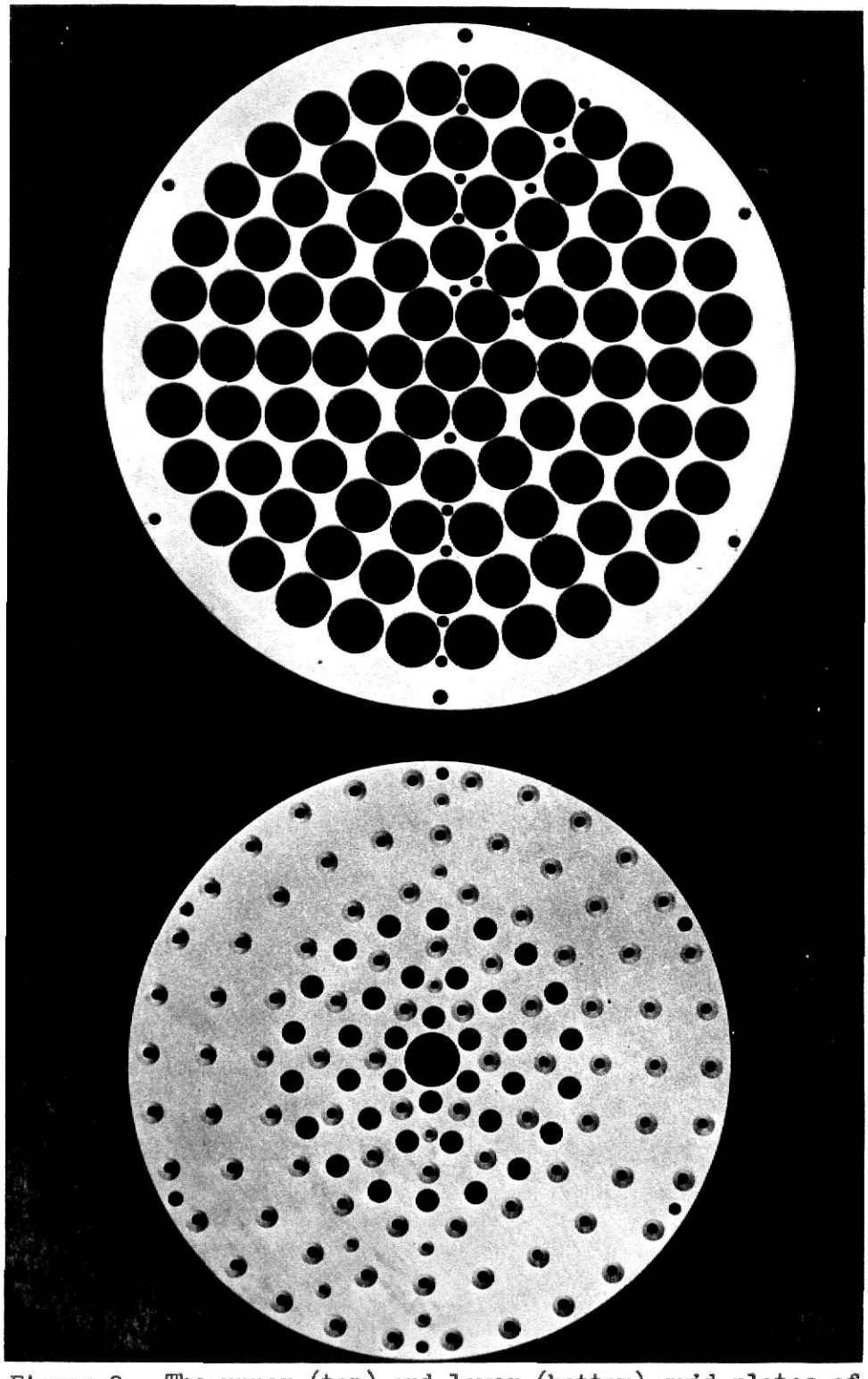

Figure 2. The upper (top) and lower (bottom) grid plates of the TRIGA.

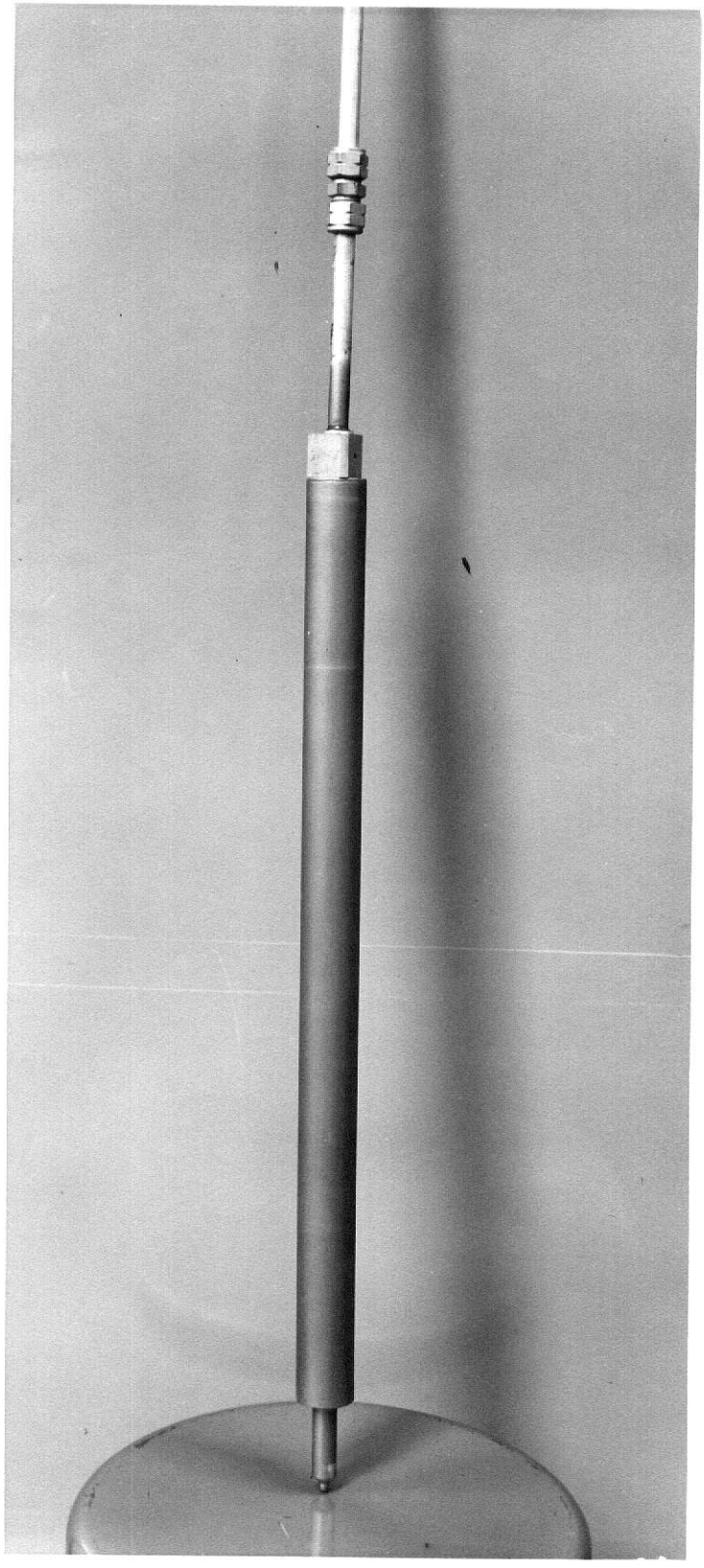

Figure 3. Exterior view of a TRIGA fuel element.

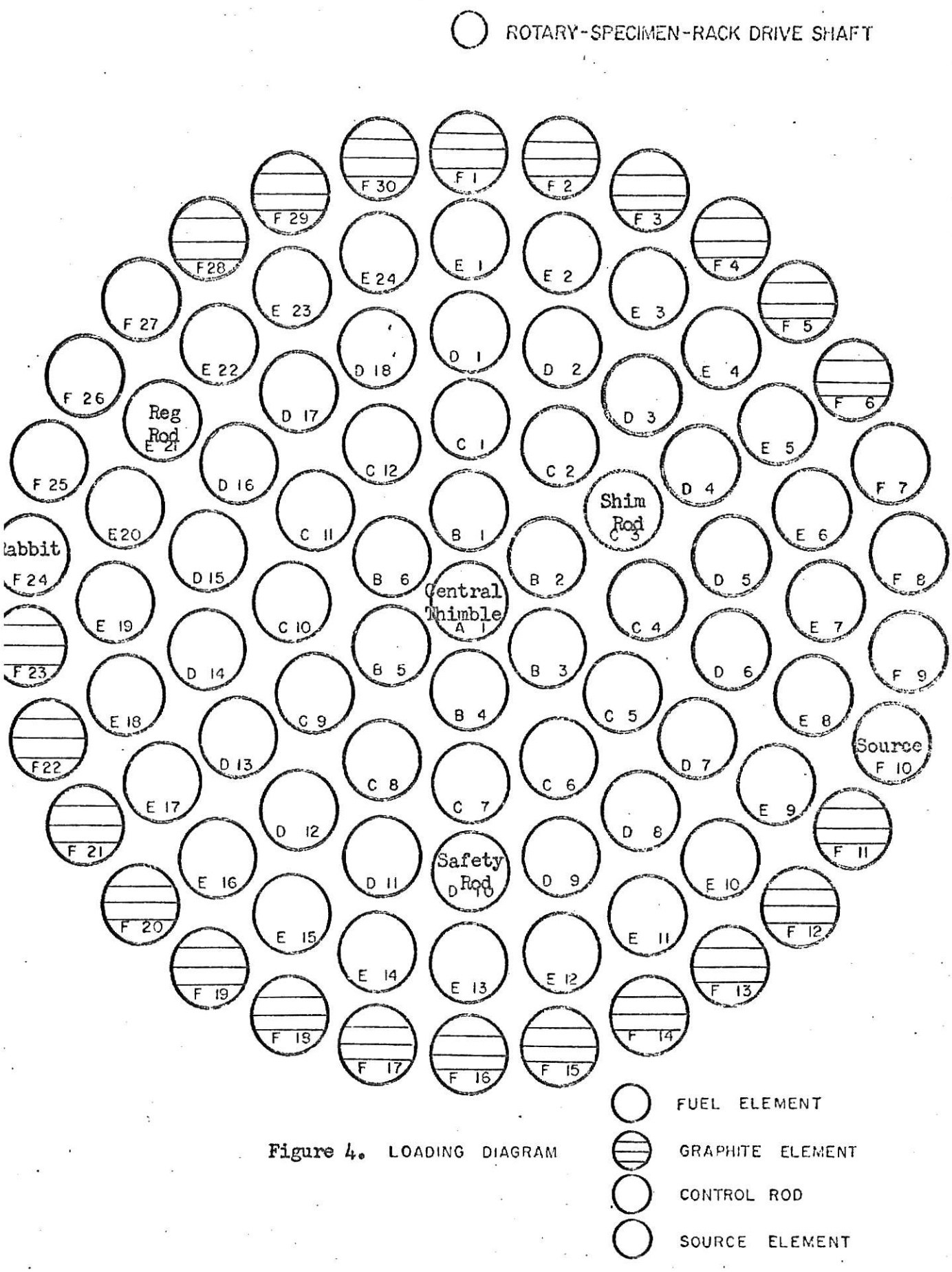

Figure 4. LOADING DIAGRAM

rods. The shim and regulating (or reg) rods are motor driven and are used for controlling the reactor in steady state operations below the 250 kilowatt licensed power of the Triga. The pulse rod is used to pulse the reactor to maximum peak power levels below 250 megawatts.

3.0 THEORY OF THE TEMPERATURE COEFFICIENT

3.1 Definitions

The effective multiplication factor, k_{eff}, is defined as the ratio of the number of neutrons produced in each generation to the total number lost by both absorption and leakage in the preceeding generation. The requirement for reactor criticality is that the number produced is equal to the number lost, i.e. $k_{eff} = 1$.

The multiplication factor is a function of many variables. For a finite system, it is expressed as

$$k_{eff} = \eta \epsilon p f P \tag{1}$$

Eta (η) is the average number of fission neutrons emitted per thermal neutron absorbed in the fuel. Symbolically, it is expressed as

$$\eta = \nu \frac{\Sigma_f}{\Sigma_a} \tag{2}$$

where

ν = average number of neutrons liberated per neutron absorbed in a fission reaction

Σ_f = macroscopic fission section for the fissile nuclide

Σ_a = total macroscopic absorption cross section in the fuel material

The fast fission factor, ϵ, is the ratio of the total number of fission neutrons produced in all fissions to the number

produced by thermal fissions alone. In thermal reactors such as the TRIGA nearly all fissions are at thermal energies, so that ϵ is approximately equal to one.

As neutrons slow down from fission energies, some of them are captured in nonfission processes. The fraction that escape capture and reach thermal energy is p, the resonance escape probability.

The fraction of thermal neutrons that are absorbed in the fuel is called the thermal utilization, f. For a heterogeneous system f is represented by

$$f = \frac{\Sigma_{a_1} V_1 \phi_1}{\Sigma_{a_1} V_1 \phi_1 + \sum_{i \geq 2} \Sigma_{a_i} V_i \phi_i} \tag{3}$$

the subscript 1 stands for the fuel region and the subscripts $i \geq 2$ denote any other region. The quantities Σ_{a_i}, V_i, and ϕ_i are the macroscopic absorption cross section, the volume, and the average flux, respectively, for the ith region.

The nonleakage probability, P, of a finite system is a measure of the probability that neutrons will not leak out of the system but instead will remain in it until they are absorbed. This probability is the product of the probabilities that the neutrons will not leak out of the system in both the fast and thermal energy ranges.

$$P = P_{th} P_f \tag{4}$$

The thermal nonleakage probability, as given by diffusion theory, is

$$P_{th} = \frac{1}{1 + L^2 B^2} \tag{5}$$

where L is the diffusion length in the medium and B^2 is the geometric buckling. The nonleakage probability during slowing down from fission to thermal energies as predicted by Fermi age theory is

$$P_f = e^{-B^2 t_{th}} \tag{6}$$

where t_{th} is the Fermi age evaluated at thermal energy.

3.2 Temperature Coefficients of the Parameters

3.2.1 Reactivity

The reactivity, ρ, for a reactor is defined in terms of k_{eff}

$$\rho = \frac{k_{eff} - 1}{k_{eff}} \tag{7}$$

so that it represents how far the reactor is from criticality.

Taking the partial derivative of Eqn. (7) with respect to temperature, results in the following equation

$$\frac{\partial \rho}{\partial T} = \frac{1}{k_{eff}^2} \frac{\partial k_{eff}}{\partial T} \tag{8}$$

Since k_{eff} is close to unity for critical systems

$$\frac{\partial \rho}{\partial T} \simeq \frac{1}{k_{eff}} \frac{\partial k_{eff}}{\partial T} \tag{9}$$

By taking the logarithm of the expression for k_{eff} and then differentiating the result one obtains

$$\frac{1}{k_{eff}} \frac{\partial k_{eff}}{\partial T} = \frac{1}{p} \frac{\partial p}{\partial T} + \frac{1}{\epsilon} \frac{\partial \epsilon}{\partial T} + \frac{1}{\eta f} \frac{\partial (\eta f)}{\partial T} + \frac{1}{P_{th}} \frac{\partial P_{th}}{\partial T} + \frac{1}{P_f} \frac{\partial P_f}{\partial T}$$

or (10)

$$\alpha_T(k_{eff}) = \alpha_T(p) + \alpha_T(\epsilon) + \alpha_T(\eta f) + \alpha_T(P_{th}) + \alpha_T(P_f) \quad (11)$$

where the alpha's (temperature coefficients) are defined by

$$\alpha_T(x) = \frac{1}{x} \frac{\partial x}{\partial T}$$

The temperature dependence of η and f is combined into one term because their dependence is more readily analyzed in this form. For heterogeneous reactors

$$\eta f = \frac{\nu \Sigma_{f\,core}}{\Sigma_{a\ core}} = \frac{\nu \Sigma_{f_1} V_1 \phi_1}{\Sigma_{a_1} V_1 \phi_1 + \sum_{i \geq 2} \Sigma_{a_i} V_i \phi_i} \quad (12)$$

The temperature coefficient of the terms in Eqn. (11) will now be analyzed for a heterogeneous reactor except that $\alpha_T(\eta f)$ will be based on a homogenization of the cell.

3.2.2 Resonance Escape Probability

The computer code RABBLE (17) was used to determine the temperature dependence of the resonance escape probability. RABBLE uses space - and lethargy-dependent slowing down sources, and the program is well suited for the computation of resonance absorption when the effects of overlapping between resonances

is significant. The reactor cell is divided into regions, and the energy range of interest is divided into extremely narrow divisions. Regional reaction rates are obtained from the slowing-down sources, first-flight transmission and escape probabilities, and interface currents. These regional reaction rates are accumulated over specified numbers of groups to yield effective cross sections.

RABBLE allows for five compositions, which can be divided into 20 regions. There can be 12 nuclides, all of which can be resonant absorbers. The total number of resonances is limited to 800. Effective cross sections and average fluxes are edited for up to 1000 intermediate groups and 25 broad groups. The code also computes the accumulated resonance absorption for each broad group.

The energy range spanned in the calculations (150-0.2eV) is the range of the resolved resonances of U-235 (19). For an intermediate group containing 69 fine groups the computing time required on the IBM 360/50 is about 2.5 minutes, so one broad group containing 20 intermediate groups was chosen to keep calculations under an hour. The intermediate group lethargy interval must be 0.331, which is too large to meet the requirement that the lethargy interval must be smaller than the maximum loss per collision with the lightest resonant material (~0.02 for U-235) which assures no within group scattering. The program was modified to handle the within group scatterings that would occur because of the coarse lethargy grid and the program was run at several temperatures so $\alpha_T(p)$ could be found.

3.2.3 Fast Fission Factor

The temperature dependence of the fast fission factor, ϵ, is mainly a function of fast neutrons. Except for the thermal expansion of the fuel rods and resulting fuel density changes and for the thermal flux flattening in the fuel at higher temperatures, which both cause decreases in the escape probability from the fuel, there is little to cause changes in ϵ. The effects named here are minor so that $\alpha_T(\epsilon)$ is extremely small compared to other effects and thus the usual assumption (4, 5, 6, 7) is to take $\alpha_T(\epsilon) = 0$.

3.2.4 The ηf Product

The temperature dependence of the ηf product was determined with a method outlined by Strawbridge (18). In this method, the reactor cell is homogenized through the use of flux and disadvantage factor weighting of the cross sections. Strawbridge compares his calculations for ηf with more rigorous calculations that were made with the code THERMOS (22). For the test cases described, his largest per cent error was less than 0.3%.

Physically, ηf is the number of fission neutrons released per thermal absorption and it is the most significant thermal parameter in criticality calculations. It can be calculated from group constants averaged over the thermal spectrum.

$$\eta f = \frac{\nu \bar{\Sigma}_{f \text{ core}}}{\bar{\Sigma}_{a \text{ core}}} \qquad (13)$$

Group cross sections are needed in the ηf calculation for the materials in the TRIGA cell. The energy dependent fluxes are needed for the averaging process and the scattering kernel and scattering cross sections are needed to calculate the fluxes.

Since the TRIGA fuel elements contain ZrH as a moderator, the energy dependent scattering cross section for the H had to be determined. The theoretical derivation of the scattering kernel for ZrH was first given by McReynolds (21). This theory assumes that the hydrogen atom acts like an Einstein oscillator (20) with a vibrational frequency $w_o = 0.130eV$ in the ZrH lattice. The calculated expression for the ZrH scattering kernel is (21)

$$\sigma_{s,ZIRK}(E_o, E, \theta) = \frac{\sigma_b}{4\pi} \sum_{n=-\infty}^{\infty} f(E_o, E, \theta) \qquad (14)$$

where $f(E_o, E, \theta) = \left(\frac{E}{E_o}\right)^{1/2} (4\pi T\lambda\gamma)^{1/2} \exp(-\gamma/A)\exp(w/2T) \cdot$

$$I_n(\gamma/B)\exp\left[-(E - E_o + w + \lambda\gamma)^2/(4T\lambda\gamma)\right] \qquad (15)$$

where σ_b = bound proton cross section

E_o = initial energy, before scattering

E = final energy, after scattering

θ = the angle of scattering

T = absolute temperature

$\gamma = E_o + E - 2(E_o E)^{1/2}\cos\theta$

For an arbitrary system w, λ, A, and B can be free parameters used to fit the data. The parameters used for ZrH are:

$$W = W_o = 0.130\text{eV}$$

$$\lambda = 1/91$$

$$A = W_o \tanh (W_o/2T)$$

$$B = W_o \sinh (W_o/2T)$$

The angular dependence of Eqn. (14) can be integrated out

$$\sigma_{s,ZIRK}(E_o, E) = \int \sigma(E_o, E, \theta)d\theta \qquad (16)$$

Then,

$$\sigma_s(E_o) = \sum_E \sigma_s(E_o, E)\Delta E \qquad (17)$$

where ΔE is the energy interval around energy E.

A computer code ZIRK was written to perform the above indicated calculations to determine the scattering kernel and scattering cross section. A description of this code is given in Appendix B. The scattering kernel output of the program is expressed as a function of velocity (in units of v_o) where $v = \sqrt{E}$.

The scattering cross section and scattering kernel ($\sigma_{s,GAKER}(i \rightarrow j)$) for the H in the water was determined from the code GAKER (28).

The energy dependent absorption, scattering, and fission cross sections of the other materials (U-235, U-238, Zr, Al, O) and the absorption cross section of H were obtained from references (20) and (23).

The cross section data were used in the calculation of group monoenergetic disadvantage factors for the cladding and

moderator. The calculation of the disadvantage factors follows the integral transport method proposed by Amouyal and Benoist (24). The geometry of the problem is given in the following figure

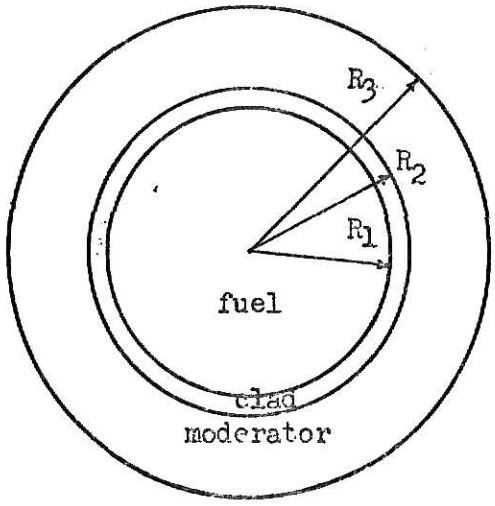

Figure 5. Fuel rod unit cell.

The subscript 1 refers to the fuel, 2 to the clad, and 3 to the moderator. The clad disadvantage factor is given by

$$\frac{\phi_2}{\phi_1} = \frac{\phi_s}{\phi_1} + \frac{\Delta\phi_2}{2\phi_1} \tag{18}$$

where ϕ_s is the flux at the fuel surface, ϕ_i is the average flux in region i and $\Delta\phi_2$ is the flux rise across the clad. Diffusion theory predicts that this flux rise is

$$\frac{\Delta\phi_2}{\phi_2} = \frac{t_2^2}{L_2^2}\frac{\Sigma_{a_1}}{\Sigma_{a_2}} \tag{19}$$

where t_2 is the clad thickness and L_2 is the diffusion length of the clad. The ratio of surface flux to average fuel flux is

determined from

$$\frac{\phi_s}{\phi_1} = 1 + \frac{\Sigma_{a_1}}{\Sigma^*_{t_1}}\left[\frac{P_c}{1 - P_c} - R_o\Sigma^*_{t_1}\right]\left[1 + \alpha\frac{\Sigma^*_{s_1}}{\Sigma^*_{t_1}} + \beta\left(\frac{\Sigma^*_{s_1}}{\Sigma^*_{t_1}}\right)^2\right] \qquad (20)$$

The asterisks indicate that the scattering and total cross sections are transport corrected for anisotropy so that

$$\Sigma^*_{s_1} = \Sigma_{s_1}(1 - \bar{\mu})$$

$$\Sigma^*_{t_1} = \Sigma^*_{s_1} + \Sigma_{a_1}$$

where $\bar{\mu}$ is the average cosine of the scattering angle in the laboratory system.

The collision probability in a cylinder, P_c, and α and β are functions of $R_1\Sigma^*_{t_1}$. Case et. al. (25) present a tabulation of P_c and α and β plots are given in Strawbridge's paper.

The disadvantage factor for the moderator is calculated as follows

$$\frac{\phi_3}{\phi_1} = \frac{\phi_2}{\phi_1} + \frac{3}{2}R_1^2\Sigma_{a_1}\left(1 + \frac{V_2\Sigma_{a_2}\phi_2}{V_1\Sigma_{a_1}\phi_1}\right)\left[\frac{2X}{3\Sigma_{a_3}(R_3^2 - R_2^2)} + \frac{1}{R_2}\left(\lambda_3 - \frac{2}{3}\right)\right] \qquad (21)$$

where X is given in terms of modified Bessel functions

$$X = \frac{(R_3^2 - R_2^2)}{2L_3R_2}\left[\frac{I_1(R_3/L_3)K_0(R_2/L_3) + I_0(R_2/L_3)K_1(R_3/L_2)}{I_1(R_3/L_3)K_1(R_2/L_3) - I_1(R_2/L_3)K_1(R_3/L_3)}\right] - 1 \qquad (22)$$

where L_3 is the diffusion length of the moderator and λ_3 is the

extrapolation length for a black cylinder. A plot of λ_3 as a function of $R_2\Sigma_{t_{r_1}}$ is given by Strawbridge (18).

Strawbridge's procedure outlined above concerns only slowing down sources in the moderator, but since the TRIGA fuel contains ZrH, slowing down sources also need to be taken in the fuel. Using the method proposed by Amouyal and Benoist, the disadvantage factor for the fuel is calculated as described in Eqn. (22). Then, a disadvantage factor for the fuel due to sources in the fuel is given by

$$\left(\frac{\phi_1}{\phi_3}\right)^* = 1 + \frac{\Delta\phi_2}{\phi_1} + \frac{3}{2} R_1^2 \frac{V_3}{V_1} \Sigma_{a_3} \left(1 + \frac{V_2\Sigma_{a_2}\phi_2}{V_1\Sigma_{a_1}\phi_1}\right) \cdot \left[\frac{2X}{3\Sigma_{a_3}(R_3^2 - R_2^2)} + \frac{1}{R_2}(\lambda_3 - 2/3)\right] \tag{23}$$

The thermal utilization due to the two sources may then be calculated as

$$f_3 = \frac{1}{1 + \frac{\Sigma_{a_1}V_1}{\Sigma_{a_3}V_2}\left(\frac{\phi_1}{\phi_3}\right)^*}$$

$$f_1 = \frac{1}{1 + \frac{\Sigma_{a_3}V_3}{\Sigma_{a_1}V_1}\frac{\phi_3}{\phi_1}}$$

Then, the disadvantage factor for the moderator due to both sources is calculated from

$$\frac{\phi_3}{\phi_1} = \frac{\Sigma_{a_1}V_1}{\Sigma_{a_3}V_3}\left[\frac{V_1Q_1f_3 + V_3Q_3(1 - f_1)}{V_1Q_1(1 - f_3) + V_3Q_3f_1}\right] \tag{24}$$

where Q_i is the slowing down power in region i and is calculated

from

$$Q_i = \xi_i \Sigma_{s_i}$$

and ξ_i is the average logarithmic energy decrement per collision.

Once the disadvantage factors are determined, the fluxes are normalized to a volume average of unity. Therefore,

$$V_1\bar{\phi}_1 + V_2\bar{\phi}_2 + V_3\bar{\phi}_3 = 1 \tag{25}$$

where the $\bar{\phi}_i$'s are the normalized fluxes and V_k is the volume fraction in region k. These disadvantage factor calculations are performed for each energy group.

The average fission and absorption cross sections for each group are calculated as follows:

$$\Sigma_{i,core} = \sum_{k=1}^{3} \left(\sum_{elements} N_{el}\sigma_{i,el} \right) V_k \phi_k \tag{26}$$

where i refers to absorption or fission, N_{el} is the number density of the elements, $\sigma_{i,el}$ is the microscropic cross section, and k subscript refers to the fuel, clad, and moderator, respectively.

The scattering cross section must contain a homogenization of both the zirconium hydride and water kernels. Redefining Eqn. (16) such that it now is in a group notation,

$$\sigma_s(i \rightarrow j) = \sigma_s(E_o, E) \tag{27}$$

where the i stands for the initial state and the j for the final state, then the scattering cross section for the core can be expressed as

$$\Sigma_{s,core}(i \to j) = \left[N_{H_{ZrH}} \sigma_{s,ZIRK}(i \to j) + \delta_{ij} \left(\sum_{el \neq H} \Sigma_{s,el}\right) v(i)\Delta v(i)\right] V_1 \phi_1 + \delta_{ij} \Sigma_{s,clad} v(i)\Delta v(i) V_2 \phi_2 + \left[N_{H_{H_2O}} \sigma_{s,GAKER}(i \to j) + \delta_{ij} \Sigma_{s,o} v(i)\Delta v(i)\right] V_3 \phi_3 \qquad (28)$$

δ_{ij} = Dirac delta function

$\Sigma_{s,el}$ = scattering cross section of the elements in the fuel except for H

$\Sigma_{s,clad}$ = scattering cross section of the cladding

$\Sigma_{s,o}$ = scattering cross section of Oxygen

As can be seen from the above, the nonmoderating elements only contribute to the diagonal of the scattering kernel and here again all contributions from the various regions are weighted by the volume fraction and average flux of the regions. Then the scattering cross section for group i is found from

$$\Sigma_{s,core}(i) = \frac{1}{v(i)\Delta v(i)} \sum_j \Sigma_{s,core}(i \to j) v(j)\Delta v(j) \qquad (29)$$

where v is velocity and Δv is the velocity interval around v.

A computer program was written to calculate the core averaged cross sections and scattering kernel. A description of this code, GROUPS, is given in Appendix C.

The cross section data and scattering kernel data were used to calculate the thermal neutron spectrum in the core. The procedure used to calculate the spectrum is given in (26) and is outlined below.

The total number of neutrons leaving a velocity interval

of a scattering material may be expressed by the following slowing down equation in terms of velocity space as

$$\Sigma_t(v)vN(v) = \int_o^{v^*} \Sigma_s(v' \rightarrow v)N(v')vdv' + S(v) \qquad (30)$$

where $N(v')$ is the velocity dependent neutron density, $\Sigma_s(v' \rightarrow v)$ is the thermal neutron scattering kernel which describes the thermal neutron scattering into each velocity interval dv, and $S(v)$ is the contribution of neutrons from higher energies which upon subsequent collisions lose energy and fall into the thermal region. The maximum cutoff velocity for the thermal region is v^*.

$S(v)$ may be expressed (26), generally, as the following summation over the elements

$$S(v) = \sum_{el} s(v)\ V_{el}\ \Sigma_{s,el} \qquad (31)$$

where

$$s(v) = \frac{2v}{1 - \alpha_{el}}\left(\frac{1}{v^{*2}} - \frac{\alpha_{el}}{v^2}\right) \qquad (32)$$

for $\alpha_{el}v^* < v < v^*$ and $s(v) = 0$ otherwise.

$$V_{el} = \text{volume fraction of the element} \qquad (33)$$

$$\alpha_{el} = \left(\frac{A_{el} - 1}{A_{el} + 1}\right)^2$$

A_{el} = mass number of the element

Rewriting Eqn. (28) in terms of a multigroup approach

gives

$$\Sigma_{tj} N_j = \sum_i N_i \Sigma_s(i \to j) + S_j \qquad (34)$$

Equation (32) may be rewritten so that an iterative procedure may be used to calculate the neutron density of the form

$$N_j^{(k)} = \frac{1}{\Sigma_{tj} - P_{jj}} \left[\sum_{i \neq j}' N_i^{(k-1)} \Sigma_s(i \to j) + S_j \right] \qquad (35)$$

where $N_j^{(k)}$ is the density for group j after the kth iteration. Using an initial guess for the density $N_j^{(1)}$, new values of the neutron densities are calculated, normalized, and checked with the previous value. This iteration procedure continues until the densities calculated agree for two iterations to within 0.001%.

The homogeneous cross sections are then calculated from the spectrum as

$$\overline{\Sigma}_k = \sum_j N_j \Sigma_k(j) \, v(j) \Delta v(j) \qquad (36)$$

where k represents either absorption or fission.

Finally, ηf is calculated from

$$\eta f = \upsilon \frac{\overline{\Sigma}_f}{\overline{\Sigma}_a} \qquad (13)$$

A computer program, SPECTRUM, written to perform the flux iteration is described in Appendix D.

These ηf calculations were performed for various temperatures

so that $\alpha_T(\eta f)$ could be determined from a plot of ηf versus temperature.

3.2.5 Thermal Nonleakage Probability

The temperature coefficient of P_{th} will be found by differentiating the analytical expression for P_{th} (Eqn. (5)).

For heterogeneous systems it's a good approximation (4, 6) to take $L^2 = L_m^2(1 - f)$ where $L_m = \sqrt{D_m/\Sigma_{a,m}}$ is the diffusion length in the moderator. The temperature coefficient is given by

$$\alpha_T(P_{th}) = - (1 - P_{th})\left[\frac{1}{L^2}\frac{\partial L^2}{\partial T} + \frac{1}{B^2}\frac{\partial B^2}{\partial T}\right] \tag{37}$$

where

$$\frac{\partial L^2}{\partial T} = (1 - f)\frac{\partial L_m^2}{\partial T} - L_m^2\frac{\partial f}{\partial T} \tag{38}$$

and

$$\frac{\partial L_m^2}{\partial T} = L_m^2\left[\frac{1}{D_m}\frac{\partial D_m}{\partial T} - \frac{1}{\Sigma_{a,m}}\frac{\partial \Sigma_{a,m}}{\partial T}\right] \tag{39}$$

The temperature coefficient of a macroscopic cross section is obtained from the following (6):

$$\frac{\partial \Sigma}{\partial T} = \frac{\partial (N\sigma)}{\partial T} = N\frac{\partial \sigma}{\partial T} + \sigma\frac{\partial N}{\partial T} \tag{40}$$

where N is the nuclear density of the material and σ refers to the microscopic thermal group cross section. N has the units of nuclei per unit volume so it can be defined as

$$N = \frac{n}{r^3} \tag{41}$$

where n is the number of nuclei and r is some characteristic dimension of the system. Then,

$$\frac{1}{N}\frac{\partial N}{\partial T} = -\frac{3}{r}\frac{\partial r}{\partial T} = -\beta \tag{42}$$

where β is the coefficient of volume expansion of the material.

In computing the derivative of σ, the usual assumptions (6) that are made are that absorption cross sections (σ_a) vary as 1/v in the thermal range and that microscopic scattering (σ_s) and transport cross sections (σ_{tr}) are temperature independent. Then it follows that

$$\alpha_T(\sigma_a) = -\frac{1}{2\bar{T}}$$

Therefore,

$$\begin{aligned} \alpha_T(\Sigma_a) &= -\left(\beta + \frac{1}{2\bar{T}}\right) \\ \alpha_T(\Sigma_s \text{ or } \Sigma_{tr}) &= -\beta \end{aligned} \tag{43}$$

The diffusion coefficient, D, as given by diffusion theory is

$$D = \frac{1}{3\,\Sigma_s} \tag{44}$$

Then, differentiating (42) and rearranging gives

$$\alpha_T(D) = \beta D \tag{45}$$

The buckling, B^2, is inversely proportional to the square of one or more of the reactor's dimensions. Therefore, B^2 can be represented as proportional to $1/r^2$ where r has the

dimensions of length. Thus,

$$\alpha_T(B^2) = -\frac{2}{r}\frac{\partial r}{\partial T} = -\frac{2}{3}\beta_r \qquad (46)$$

where β_r is the volume coefficient of expansion of the reactor as a whole. In liquid moderated systems this coefficient is very nearly the same as that of the moderator (7).

Substituting Eqns. (46), (45), (39), and (38) into Eqn. (35) gives

$$\alpha_T(P_{th}) = -(1 - P_{th})\left[\frac{4\beta_m}{3} + \frac{1}{2T} - \frac{1}{(1-f)}\frac{\partial f}{\partial T}\right] \qquad (47)$$

The temperature dependence of f can be extracted from the $\alpha_T(\eta f)$ data by weighting the absorption cross section in the fuel with the calculated spectrum and with the fuel volume fraction so that Eqn. (3) can be used for the calculation of f.

3.2.6 Fast Nonleakage Probability

The temperature coefficient of the fast nonleakage probability, P_f, will be found by analyzing the analytical expression for P_f (Eqn. 6). The temperature coefficient of P_f is

$$\alpha_T(P_f) = -B^2 t_{th}\left[\frac{1}{t_{th}}\frac{\partial t_{th}}{\partial T} + \frac{1}{B^2}\frac{\partial B^2}{\partial T}\right] \qquad (48)$$

The Fermi age is defined by

$$t(E) = \int_{E_o}^{E} \frac{D_m(E)}{\xi \Sigma_{s,m}(E)}\, dE \qquad (49)$$

where E_o is the energy of the source of neutrons and ξ is the

average logarithmic energy decrement per collision. Since D_m is proportional to $1/\Sigma_{s,m}$ it can be seen that t is proportional to $1/N_m^2$. Hence,

$$\alpha_T(t) = N_m^2 \frac{\partial(\frac{1}{N_m^2})}{\partial T} = 2\,\beta_m \qquad (50)$$

Then, substituting Eqns. (50) and (46) into Eqn. (48) gives

$$\alpha_T(P_f) = -\,B^2\, t_{th} \left[\frac{4}{3}\,\beta_m\right] \qquad (51)$$

3.3 Results and Discussion

The total temperature coefficient of reactivity was found by summing the temperature coefficients of all the terms comprising k_{eff}. The resolved resonance region of U-235 was the energy range considered by RABBLE in the calculations for the resonance escape probability of the KSU TRIGA Mark II. In this range (150-0.2 eV) there are 197 cross section resonances of U-235 and 18 resonances in the cross sections of U-238 (19). The program was run with several input fuel temperatures chosen to span the temperature range of interest and the results of the calculations are given in Fig. 6. The temperature coefficient of p is found from

$$\alpha_T(p) = \frac{1}{p}\frac{\Delta p}{\Delta T}$$

and it is plotted in Fig. 8.

The programs ZIRK, GROUPS, and SPECTRUM were used in the

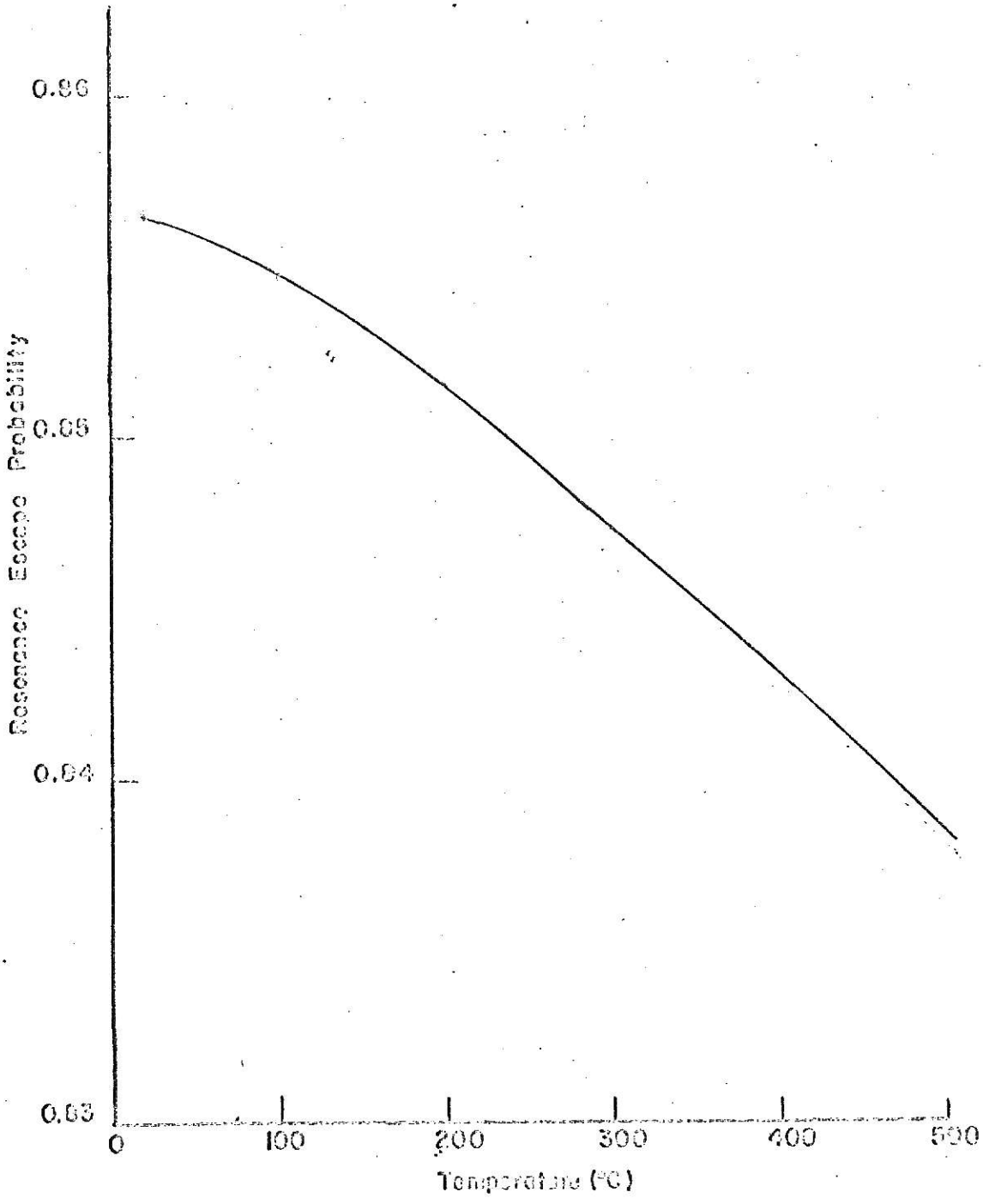

Figure 6. Resonance escape probability as a function of temperature as calculated by RABBLE for the KSU TRIGA Mark II.

calculation of the temperature dependence of ηf. Figure 7 shows the results of the calculations. The temperature coefficient is found from

$$\alpha_T(\eta f) = \frac{1}{\eta f} \frac{\Delta \eta f}{\Delta T}$$

and this also is plotted in Fig. 8.

The temperature coefficients of the nonleakage probabilities were found as described in 3.2.5 and 3.2.6. The temperature coefficients of P_{th} and P_f are plotted in Fig. 8.

The coefficients combine in a manner such that the total temperature coefficient doesn't change considerably over the temperature range analyzed. The average value of the coefficient over the range from 60°C to 450°C is $8.66 \times 10^{-5} \Delta k/k°C$ evaluated at 215°C. The magnitude of the temperature coefficient changes only 11% from the average at the extremes of the range. Converting to dollar units, the average value of the temperature coefficient is

$$\alpha_T(k_{eff}) = 1.096 \ \$/°C$$

The value reported (1) for the TRIGA is 1.52 $\$/°C$ and experimental values of this coefficient are given in the following section.

The slight temperature dependence of the coefficient shown in Fig. 8 was also observed experimentally by Stauder (16) in his work on the KSU TRIGA Mark II.

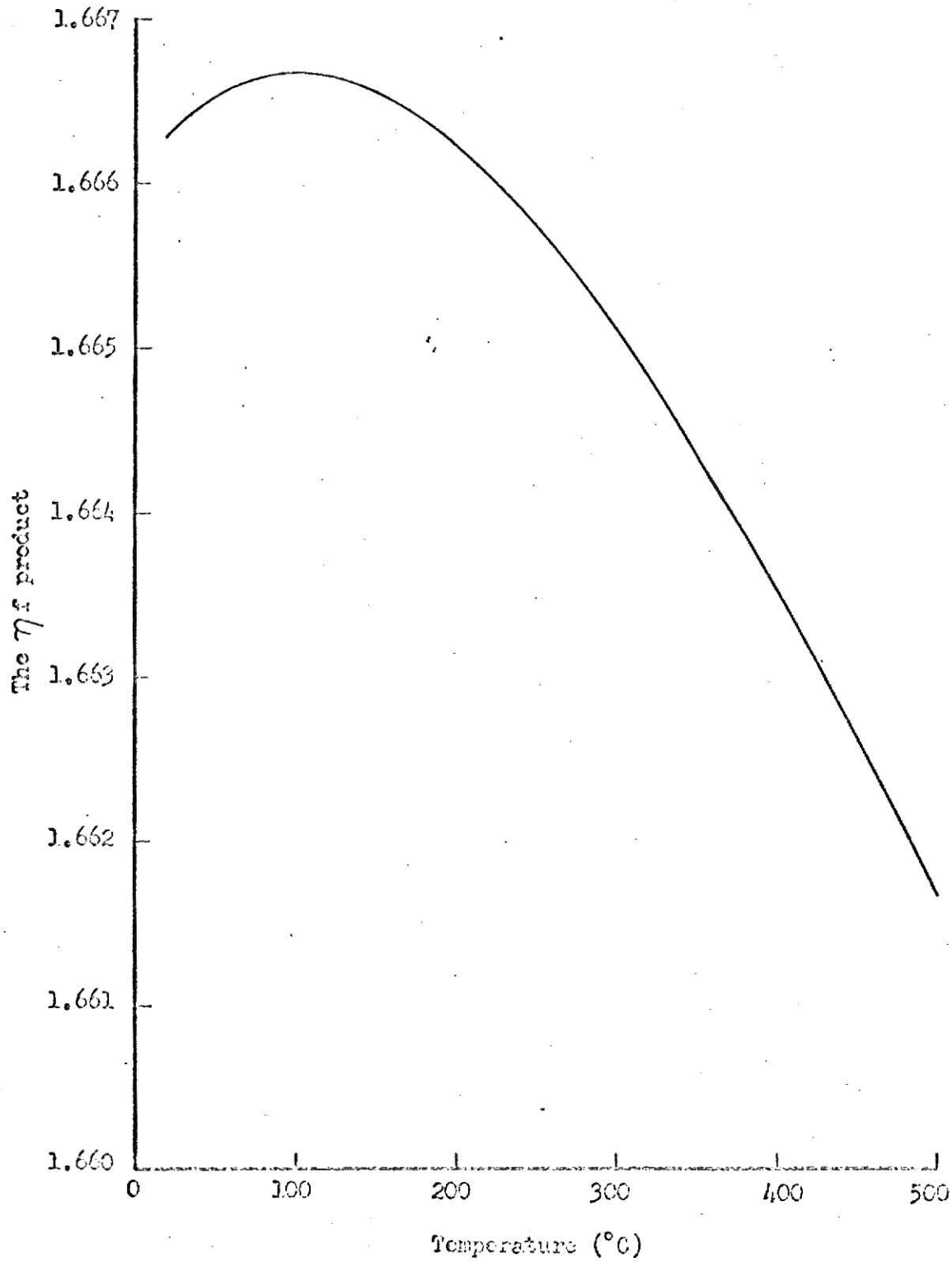

Figure 7. The temperature dependence of the ηf product of the Kansas State University TRIGA Mark II Nuclear Reactor.

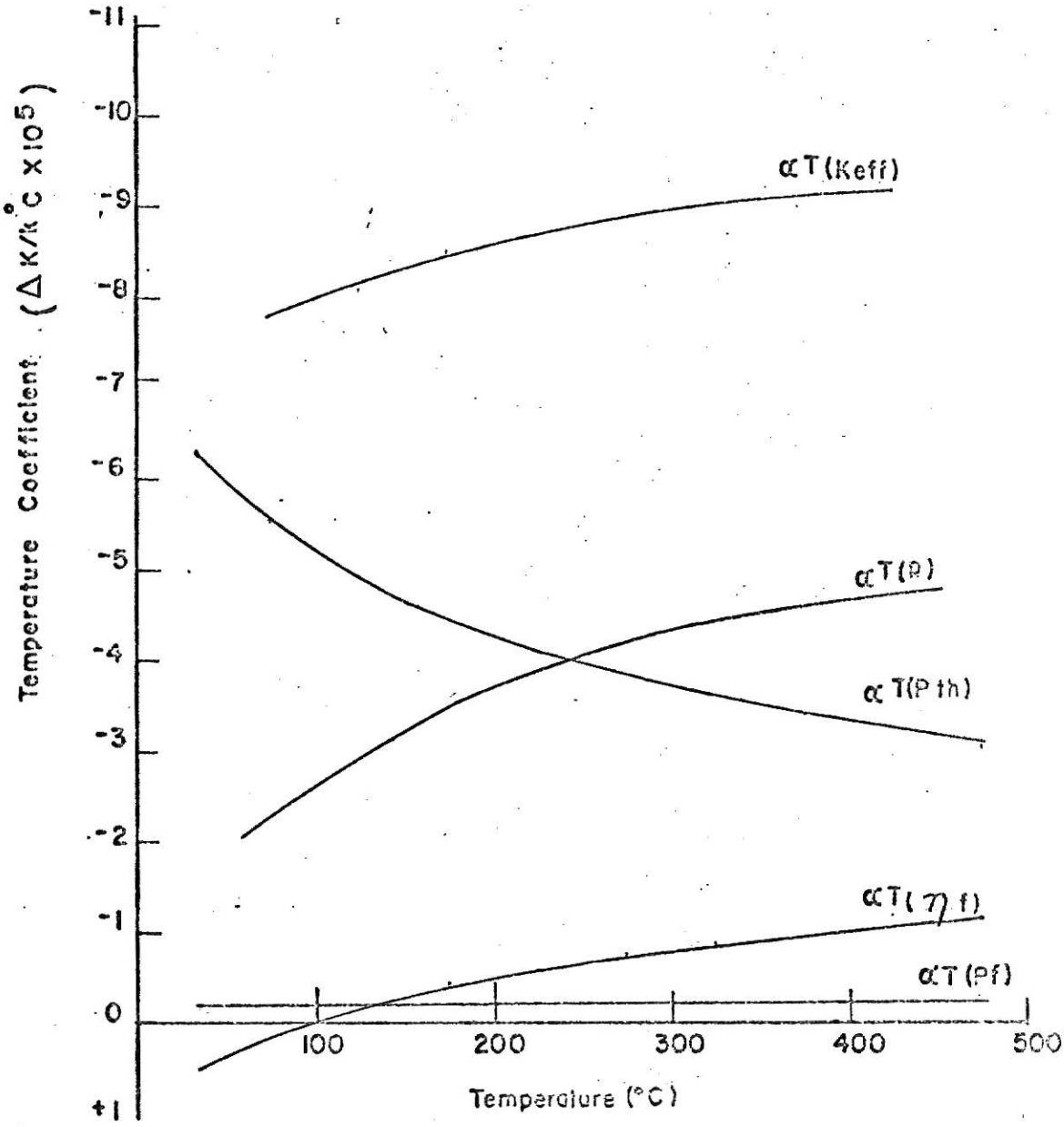

Figure 8. The total temperature coefficient curve showing the contributions from all the parameters of k_{eff}.

4.0 EXPERIMENTAL DETERMINATION OF THE TEMPERATURE COEFFICIENT.

4.1 Experiment Design

4.1.1 Reactor Licensing

The technical specifications of the reactor operating license of KSU's TRIGA (11) limit the maximum fuel temperature to 450 °C and place an upper bound of $2 on reactivity insertion into the core.

Initial calculations showed that the sample size needed to note a measureable reactivity change due to heating a sample by 100 °C was approximately the size of a fuel element. In order to elevate the temperature of this sample, it was decided to use nuclear heat. An insulation applied to the exterior of the element would restrict the flow of heat from the element and elevate its temperature with respect to the normal uninsulated condition. The largest opening in the top grid plate (see Fig. 2) is the central thimble hole. Its I.D. is 1.515 inches while the O.D. of a fuel elements is 1.475 inches. Thus, there is only a 0.020" radial gap which places a limit on the thickness of insulation for an element placed in the central thimble.

The insulation chosen was ScotchTite brand heat shrinkable tubing with 0.002" wall thickness made by the 3M Company. It is easily applied to an element with a heat gun and does not corrode or damage the element in any way. Several layers can be applied without wrinkles between layers. It was later determined that the insulation deteriorated and failed from radiation damage after about 750 kilowatt hours of operation.

In order to perform this experiment, a hazards analysis had to be performed to show that the maximum fuel temperature of an insulated element in the central thimble would not exceed the 450°C limitation. Also the reactivity limitation had to be considered. The worth of an element in the B ring, adjacent to the central thimble was determined to be $1.57. Since the insertion of a fuel element in the central thimble would depress the flux in the central thimble, the worth of an element in this position would be considerably less than the $2 limit and the reactivity limitation did not restrict the experiment.

The hazards analysis submitted to the AEC with the license application to perform the experiment is contained in Appendix A. The license application was approved by the AEC but the experiment was limited to operating below the first to occur of 100 kW or a temperature of 350°C in the element in the central location.

4.1.2 Insulated Instrumented Element

A cold clean instrumented fuel element, number TC 2744E was available for use in this experiment. It contains three thermocouples located on the centerline, an inch above the centerline, and an inch below the centerline of the element as is shown in the internal diagram of the element (Fig. 9). Figure 3 shows the exterior of the element and Fig. 10 shows the element as it was used in the reactor. Three layers of the insulation were all that could be applied to the element with a

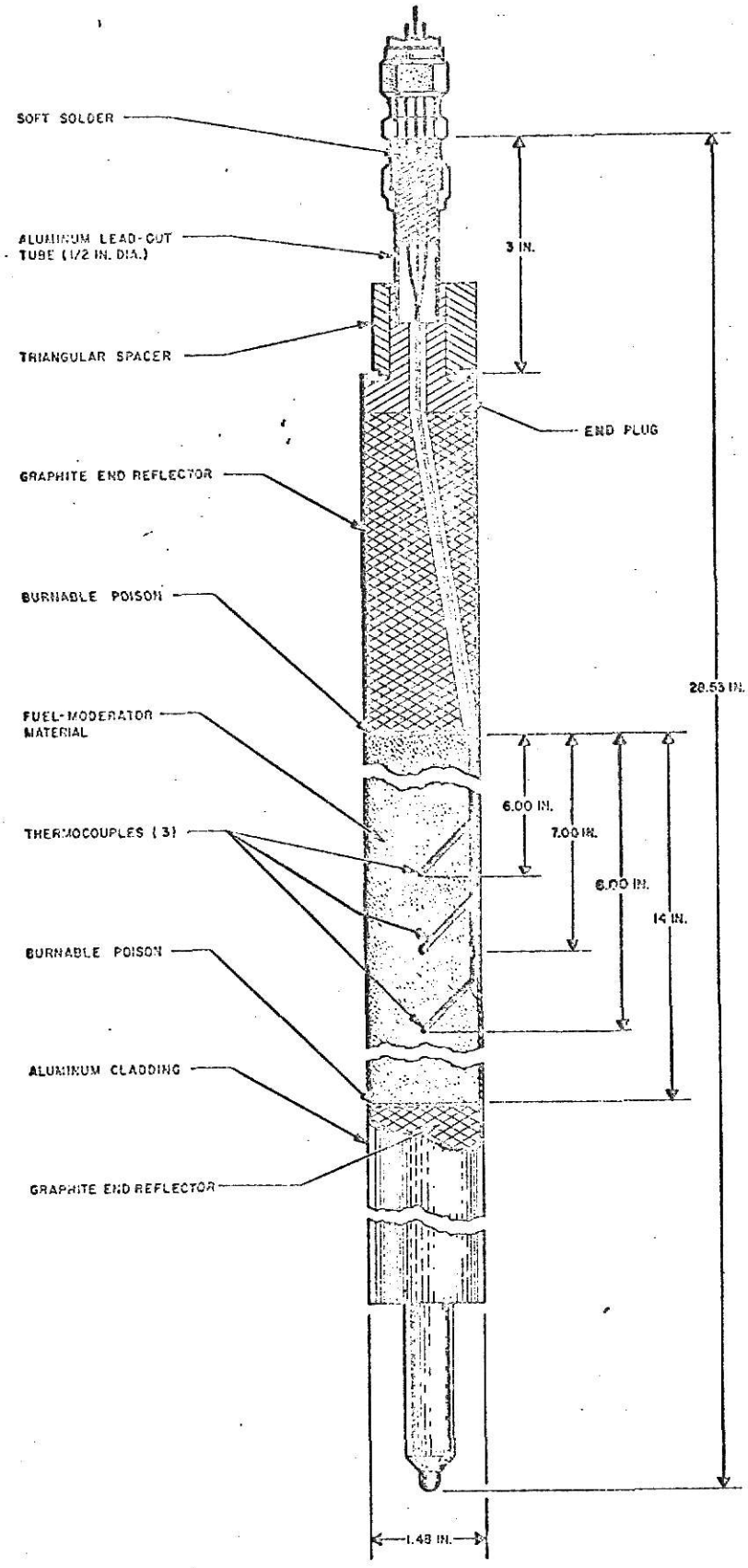

Fig. 9. TRIGA instrumented fuel element

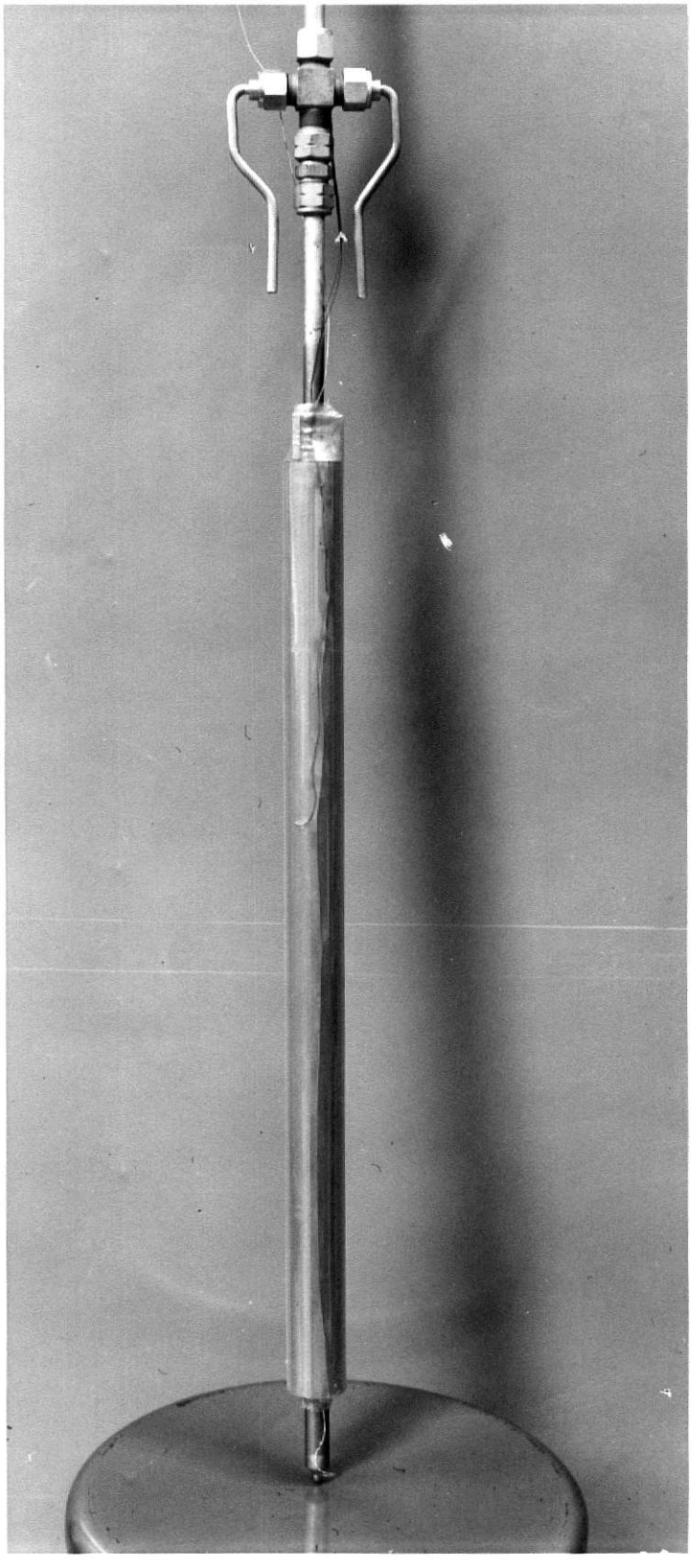

Figure 10. The insulated instrumented element as it was used in the experimentation.

stripping wire beneath the insulation and still enable the element to be fit into the central thimble. The apparatus on the aluminum conduit above the element was needed to support the element on the top grid plate at the same elevation as the other elements. This was necessary because the bottom grid plate, which supports all other elements has a hole in it in the central thimble position which allows the central thimble tube to pass through the grid plate.

4.2 Reactor System Initilization

4.2.1 Approach to Critical

An approach to critical experiment was performed because the presence of an element in the central thimble constituted an unknown critical configuration for the reactor.

The central thimble tube was removed from the core. The elements from positions F-7, F-8, E-4, E-5, E-6, and E-7 were removed from the core and then the insulated element was placed in the central thimble. The approach to critical experiment as described in (1) was performed to find the critical configuration.

The elements from the F ring were left in the storage rack since excess reactivity limitations described in the reactor license would have been exceeded if they were left in the core.

4.2.2 Power Calibration

A power calibration was necessary because the removal of elements F-7, F-8, and F-9 from the core had shifted the flux

slightly so that the linear and log power recorder on the reactor console were no longer calibrated to the true power. A calorimetric power calibration was performed using a thermistor to measure the bulk water temperature with the log recorder set at 30 kW. This calibration determined that the true power was 30 kW, as indicated by the log recorder. The linear recorder was reading a higher power, thus the position of its fission chamber was adjusted so that it indicated the correct power for this reactor configuration.

4.2.3 Control Rod Calibration

Control rod calibrations were also required for this new reactor configuration. A zero power check of the control rod calibrations was performed by making the reactor critical at several different positions of the shim and reg rods. Calibration curves for the regular configuration (Figs. 11 and 12) were used in the check. The range over which the sum of the worths of both rods gave a reproducible total worth was found to be from 250 to 550 for the reg rod and from 500 to 620 for the shim. Since these control rod calibration curves gave consistent critical worths, they were also used in the above mentioned ranges as the calibration curves for the new reactor configuration.

4.3 Experimental Equipment and Procedure

4.3.1 Steady State Method

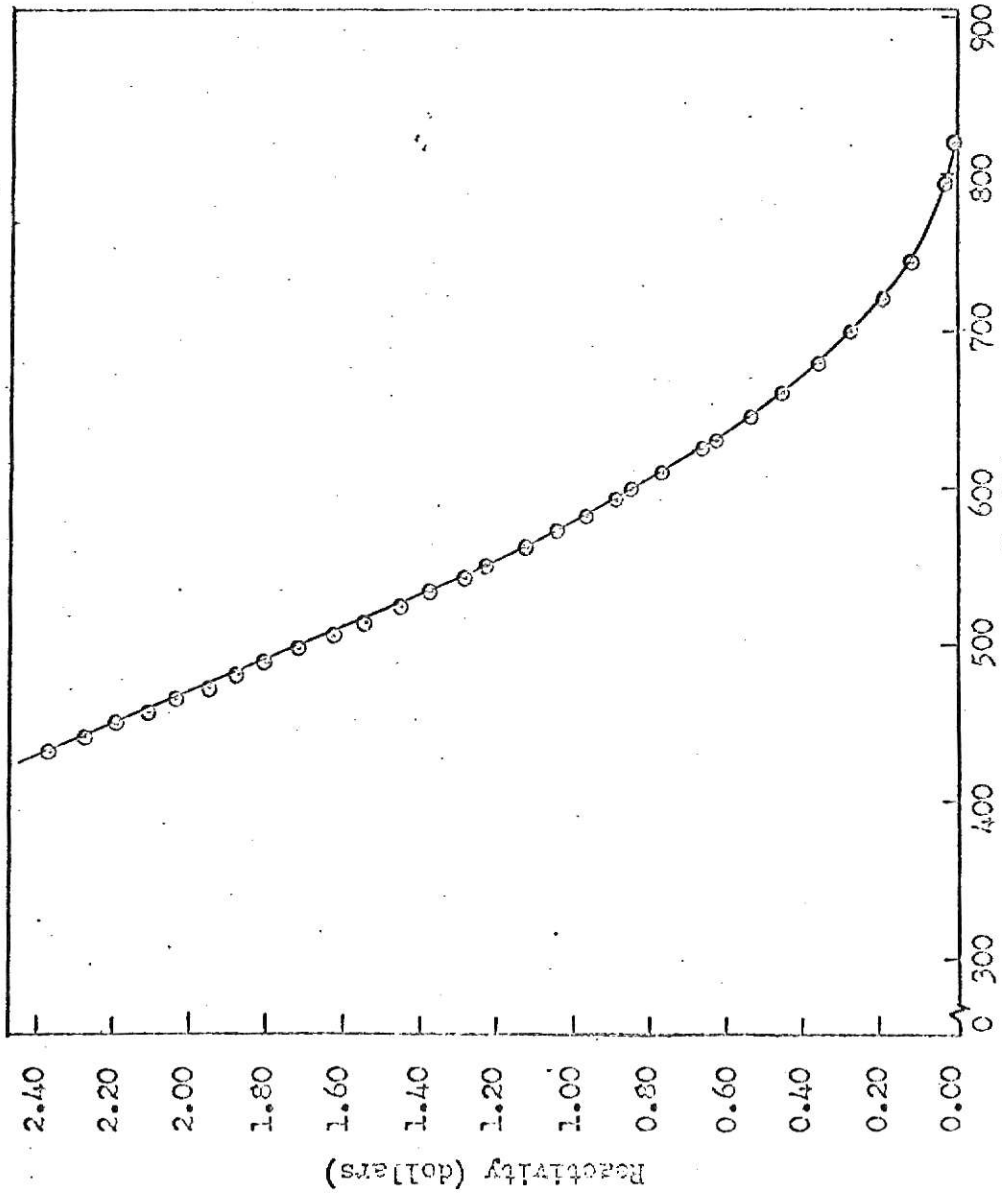

Figure 11. Shim rod calibration curve.

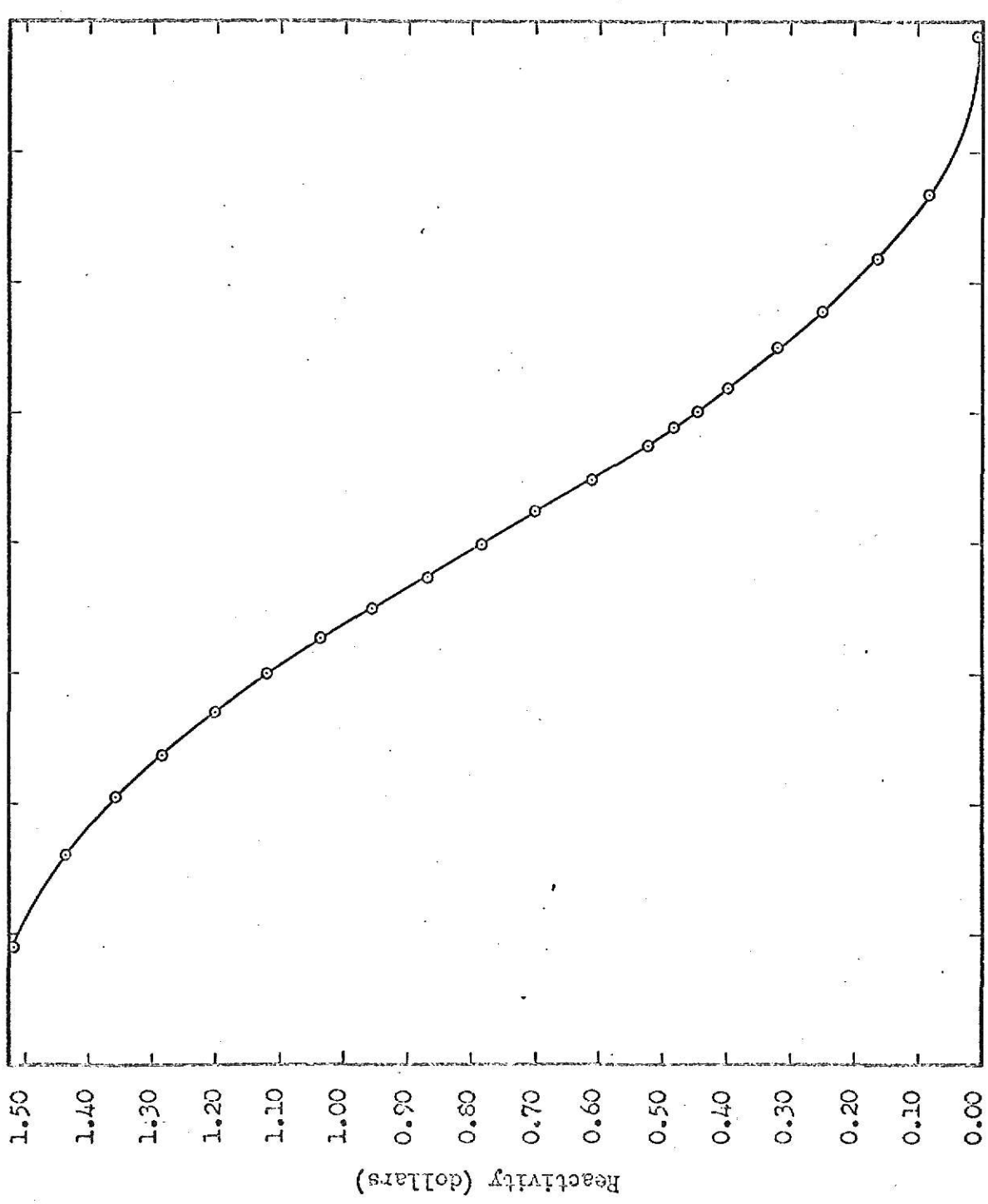

Figure 12. Reg rod calibration curve.

In order to note the effect of temperature on reactivity while at steady state, the following procedure was used. First the reactor was brought to criticality at zero power. The control rod positions were recorded and the temperature of the central thimble element and the instrumented element in core position B-5 were measured using a Leeds and Northrup potentiometer. The water temperature was monitored by a thermistor. The same data were taken at 90 kW. This procedure was repeated twenty times.

The above data were taken for three conditions, with the insulated element, bare element, and the element usually in position B-3 inserted in the central thimble. The temperature effect on reactivity caused by the increased temperature of the insulated element can be found by differencing the bare and insulated reactivity data. Data with the B-3 element in the central location were taken as a check on the method. Since the experiment could not be performed again, once the element was stripped of its insulation, data were taken on the B-3 element for comparison with the insulated element data to see if reasonable values of the temperature coefficient were being obtained by this method. The B-3 element was used because it is an instrumented element and also because of the instrumented elements available its U-235 mass most closely matched the mass of U-235 in TC 2744E.

4.3.2 Transient Method

The transient method involves dropping the reactor power

from 90 kW to 10 kW very quickly and recording temperatures and control rod positions until steady state is reached again at 10 kW. The traces of power and temperature would ideally look as follows:

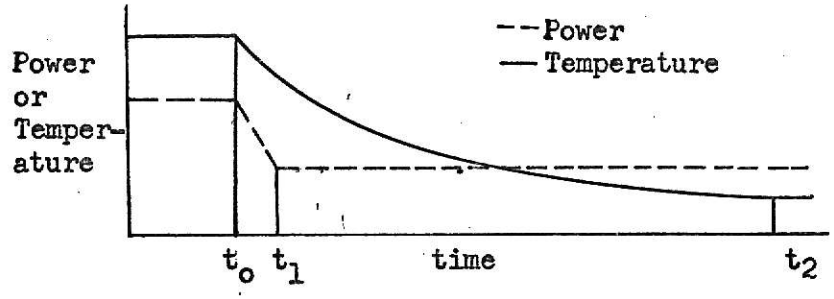

Fig. 13. Ideal temperature and power traces.

The traces of the temperatures in the central thimble and in the B-3 element as well as a power trace were recorded on a brush recorder. The power was measured with an ionization chamber and is used in the data analysis as a time initilization for the temperature data. The recorder and power indicating devices are shown in Fig. 14 and a schematic of the system is shown in Fig. 15.

The power was dropped by driving the shim rod into the core and keeping the reg rod position constant. The shim rod was continually adjusted to maintain criticality and its positions were recorded as a function of time until steady state was again reached. Shim rod position versus time data were then available from the strip chart paper and temperature versus time data were available, therefore, reactivity versus temperature data

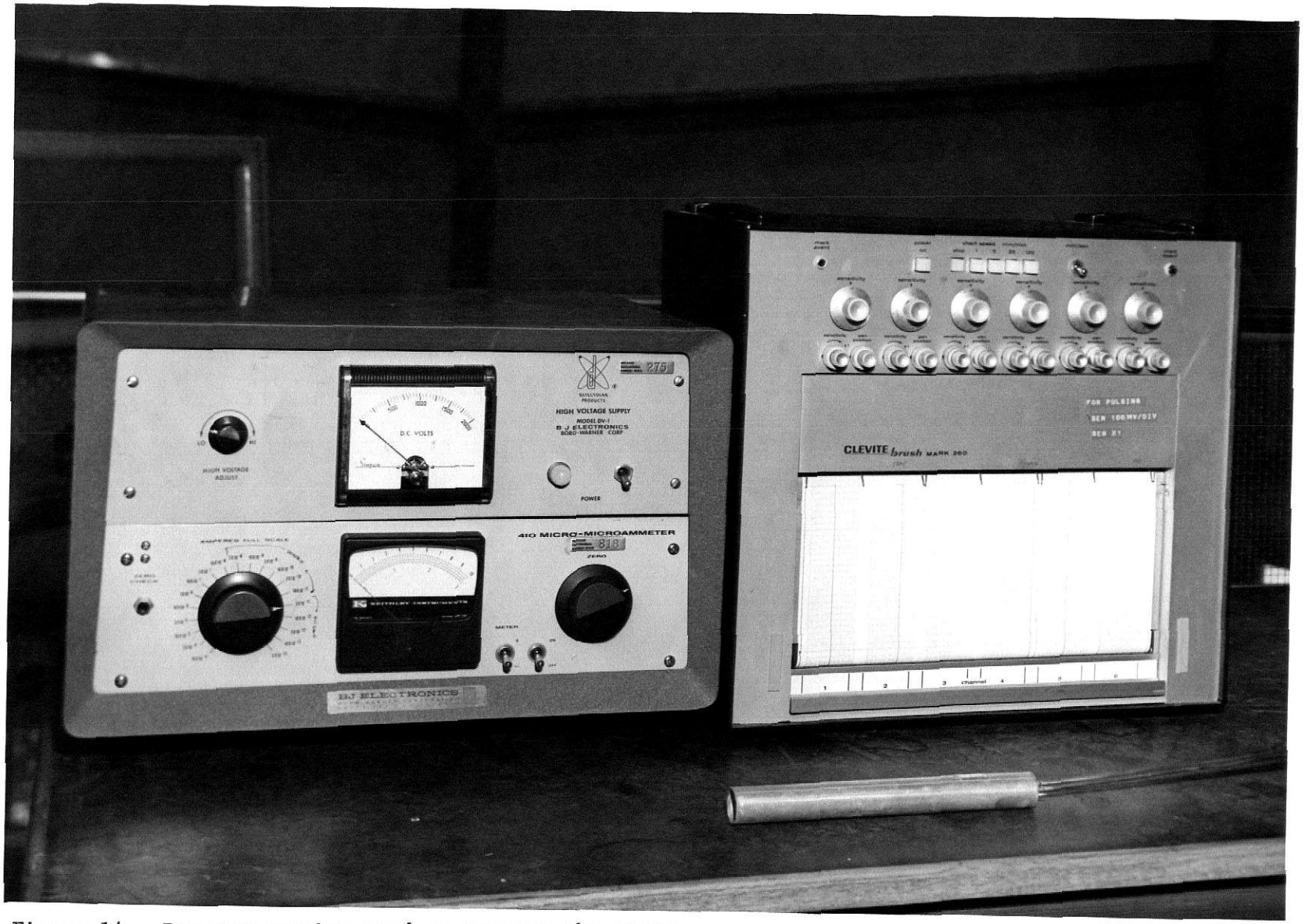

Figure 14. Instrumentation used to measure the power.

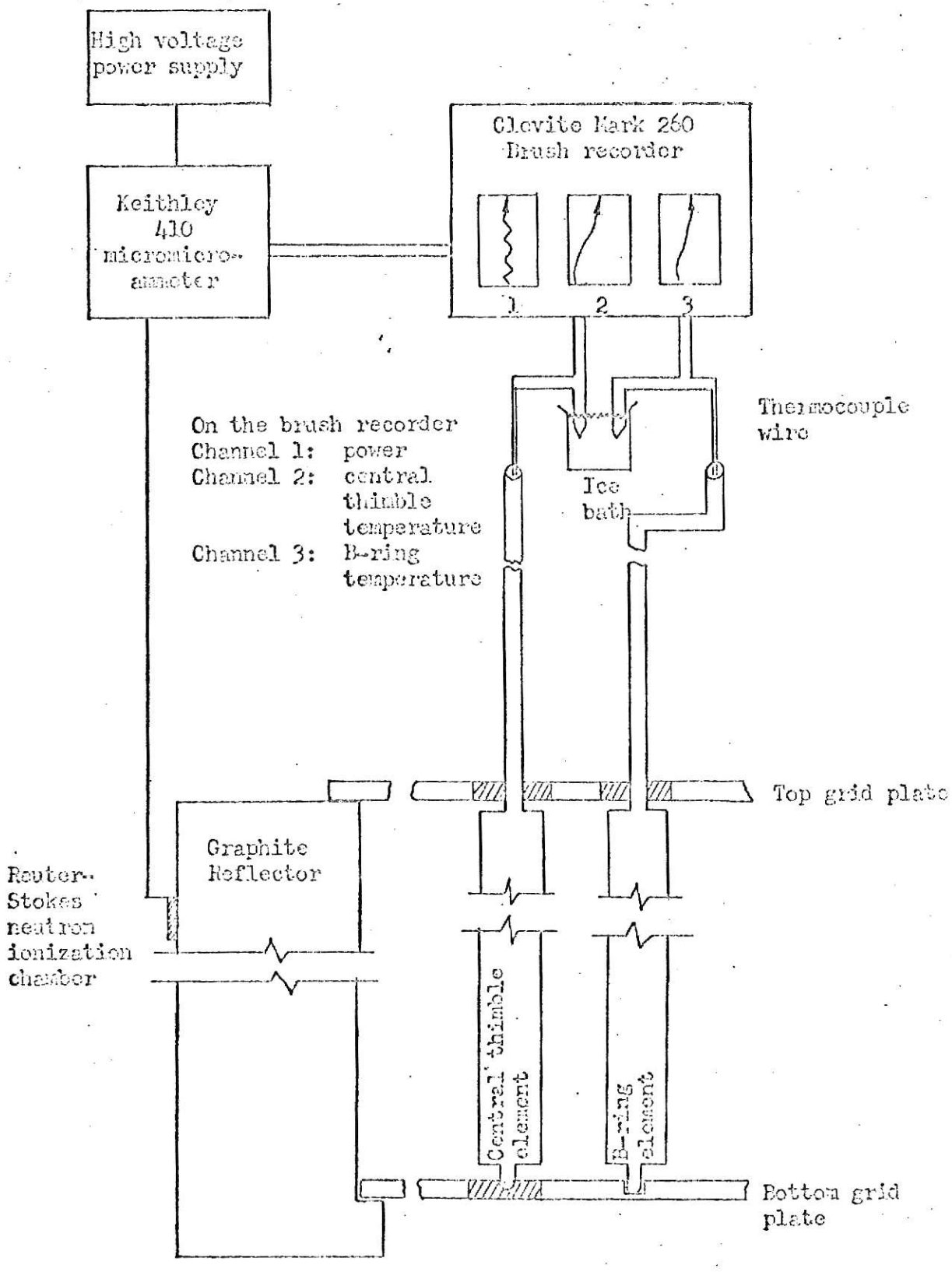

Figure 15. Instrumentation diagram of the equipment used to measure the transient temperature and power data.

were recorded.

The above procedure was repeated twenty times with first the bare and then the insulated element in the central thimble.

4.4 Results and Discussion

The reactivity loss created by the raising of the temperature of the single element can be found from the steady state data. The average values of temperature and of the reactivity differential between zero power and 90 kW for each of the three cases is given in Table 1. (NOTE: The temperatures reported here, as well as all other temperatures in this paper, are the temperatures above the water temperature. The water temperature changed during experimentation but the effect of this change on the temperature of the elements has been shown insignificant.

Table 1

Steady State Differential Control Rod Worths

Element in central thimble	Temp. at 90kW (^{o}C)	Reactivity change from 0 power to 90 kW ($\not$)
Insulated TC 2744E	237.7 $\pm$ 9.7	-87.51 $\pm$ 2.04
Bare TC 2744E	125.6 $\pm$ 5.0	-84.01 $\pm$ 1.39
B-3	138.7 $\pm$ 4.4	-84.56 $\pm$ 1.22

The standard deviations listed for the above temperatures include the statistical uncertainty of the data and a $\pm$2.3^{o}C uncertainty associated with the chromel-alumel thermocouple

wire (28).

The average temperature coefficient for the element over the temperature range from T_{ins} to T_{bare} can be found from the above data by calculating

$$\alpha_T = \frac{\rho_{ins} - \rho_{bare}}{T_{ins} - T_{bare}}$$

The average coefficient found by comparing the data taken with element TC 2744E is $\alpha_T = -0.0312 \pm 0.0223$ ¢/°C. The coefficient found by the comparison of the insulated element and the bare B-3 element data is $\alpha_T = -0.0298 \pm 0.0243$ ¢/°C. The standard deviations reported are mostly due to the uncertainty in the reactivity data. The temperature data uncertainty contributes only about 1% of the uncertainty in the average temperature coefficients.

The temperature and power traces of a typical power drop transient are shown in Fig. 16. The central thimble element temperature versus control rod reactivity data for the first four runs of the insulated and bare cases is plotted in Figs. 17 and 18. However, to put the data on a comparable basis, the reactivity data must be analyzed with respect to the average core temperature. The B-ring element is used as a standard because the same B-ring temperatures in both the insulated and bare cases will insure that the rest of the core is in a corresponding condition. Then, the only perturbation in the core is due to the increased temperature in the central position when it is occupied by the insulated element. A plot of the B-ring temperatures for

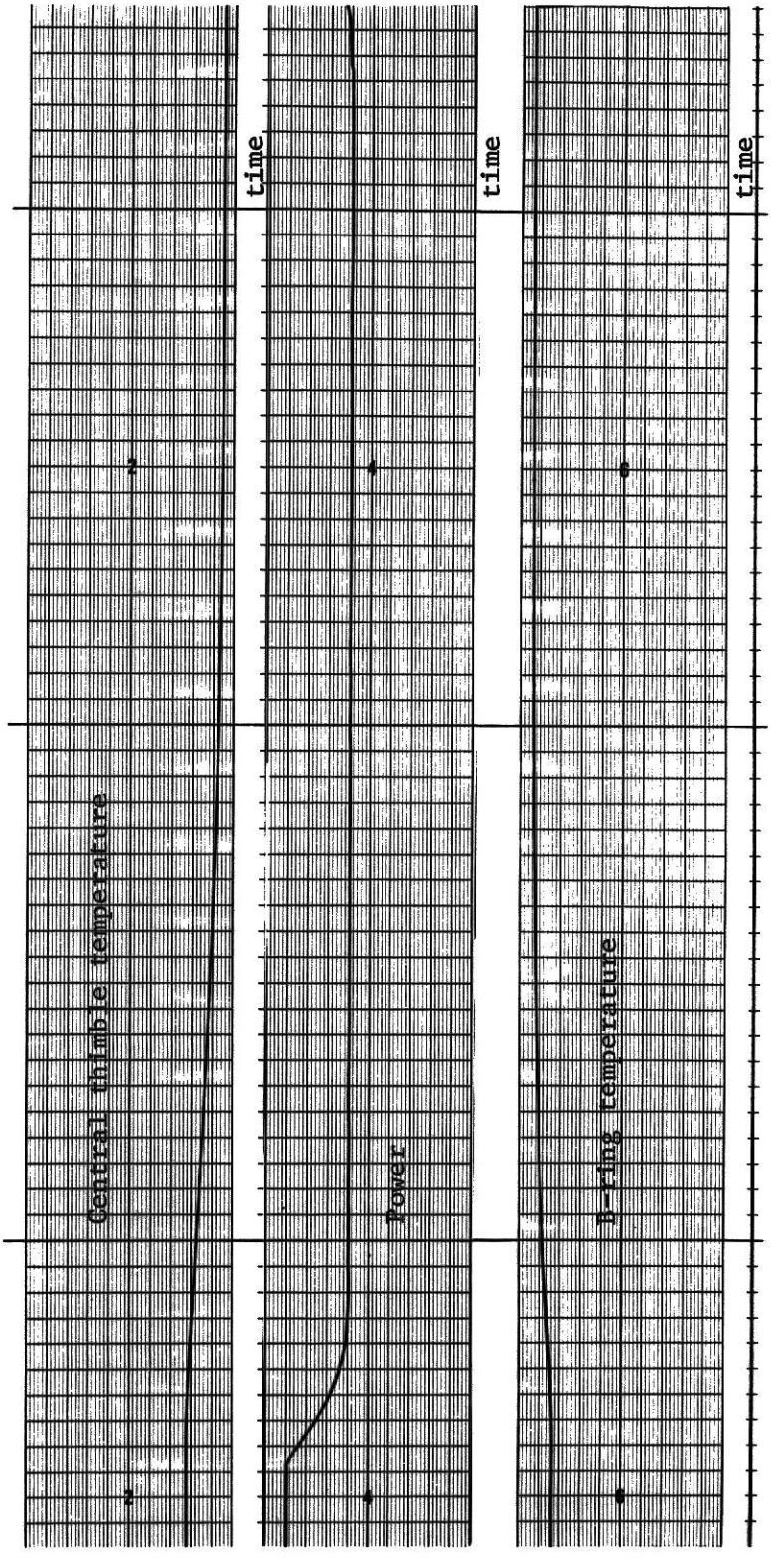

Figure 16. Temperature and power traces of a typical transient run.

both cases versus control rod reactivity is given in Fig. 19. The error bars given in the figure show the statistical uncertainity of the data. The total uncertainty in the data points will also include a $\pm 2.3^{\circ}C$ uncertainty associated with the precision of the thermocouple wire.

The reactivity needed to keep the reactor critical after the power drop is a function of the delayed neutron effects, the temperature effects, and the control rod effects. The delayed neutrons, resulting from an asymptotic precursor concentration at 90 kW, cause the power to decrease more slowly than it would with a precursor concentration at 10 kW, while the initial control rod motion and the temperature drop cause the power to decrease. As the transient effect of the delayed neutrons dies out, and as the fuel cools, the reactivity is compensated for by more control rod motion. In the core center where the measurements were made, leakage has little effect on the reactivity so it is a good assumption that to keep the reactor critical the control rod motion (positive reactivity effect after initial drop) and the temperature effect (positive effect due to fuel cooling) just balance the transient delayed neutron effect.

The reactor kinetics of the delayed neutron effect can be analytically described. The flux after a step insertion of reactivity, considering only one delayed group is given by (6)

$$\phi(t) = \frac{\alpha_2(\alpha_1 + \lambda)\phi_o}{\lambda(\alpha_2 - \alpha_1)} e^{\alpha_1 t} + \frac{\alpha_1(\alpha_2 + \lambda)}{\lambda(\alpha_1 - \alpha_2)} \phi_o e^{\alpha_2 t} \qquad (52)$$

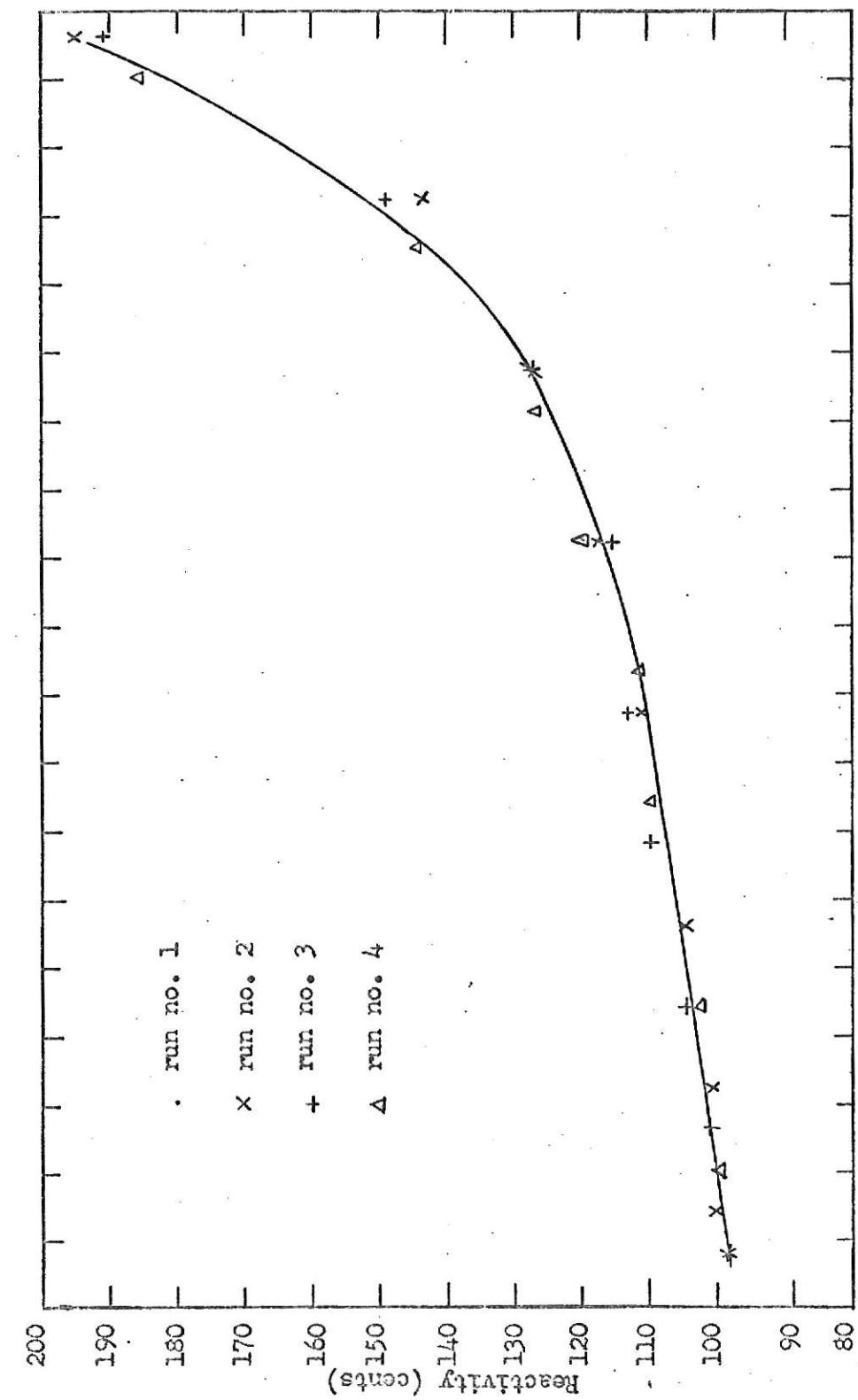

Figure 17. The worth of the shim rod remaining in the core plotted versus the temperature of the insulated element following the power drop for the first four runs with the insulated element in the central thimble position.

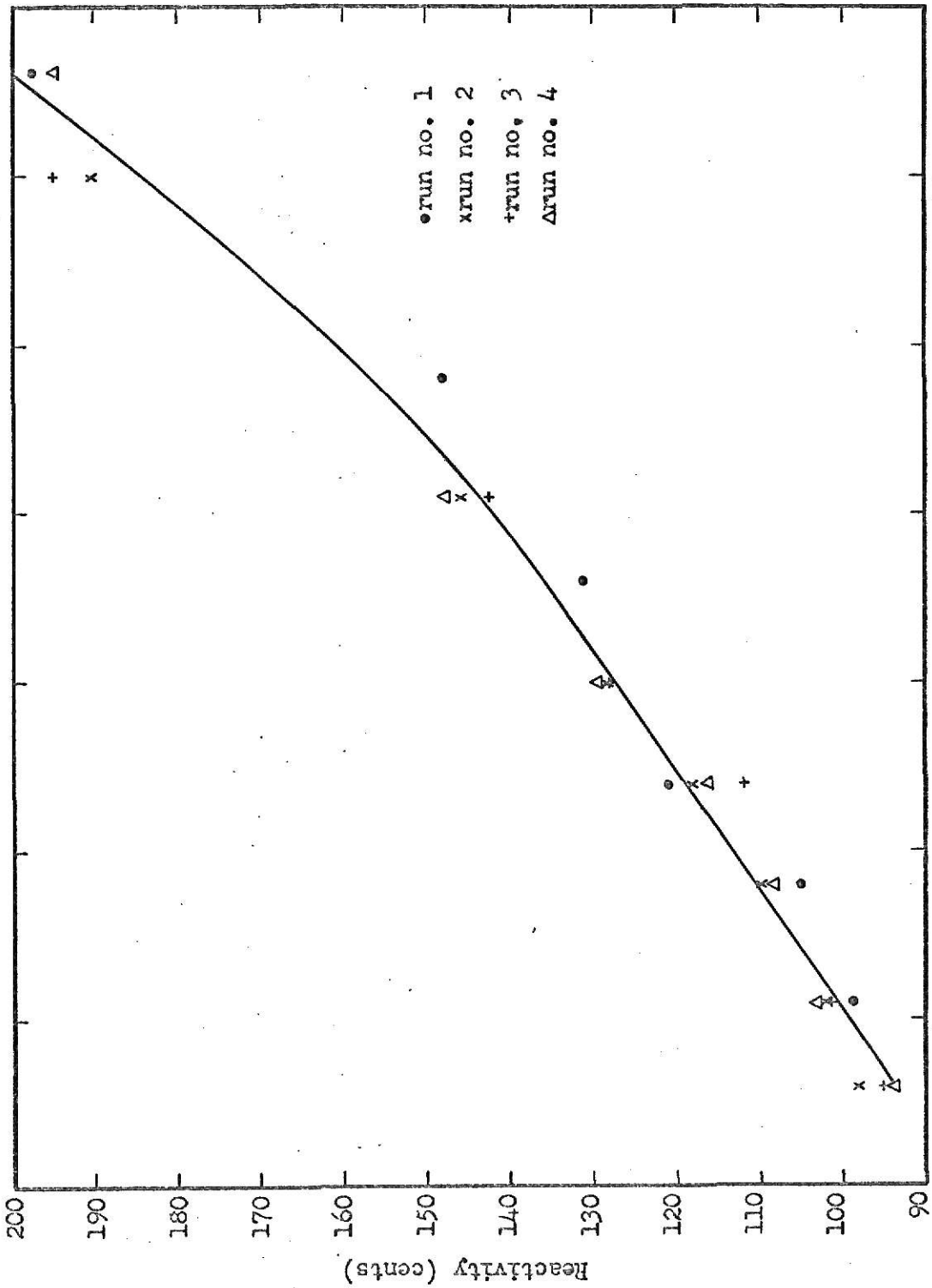

Figure 18. The worth of the shim rod remaining in the core plotted versus the temperature of the bare element following the power drop for the first four runs with the bare element in the central thimble position.

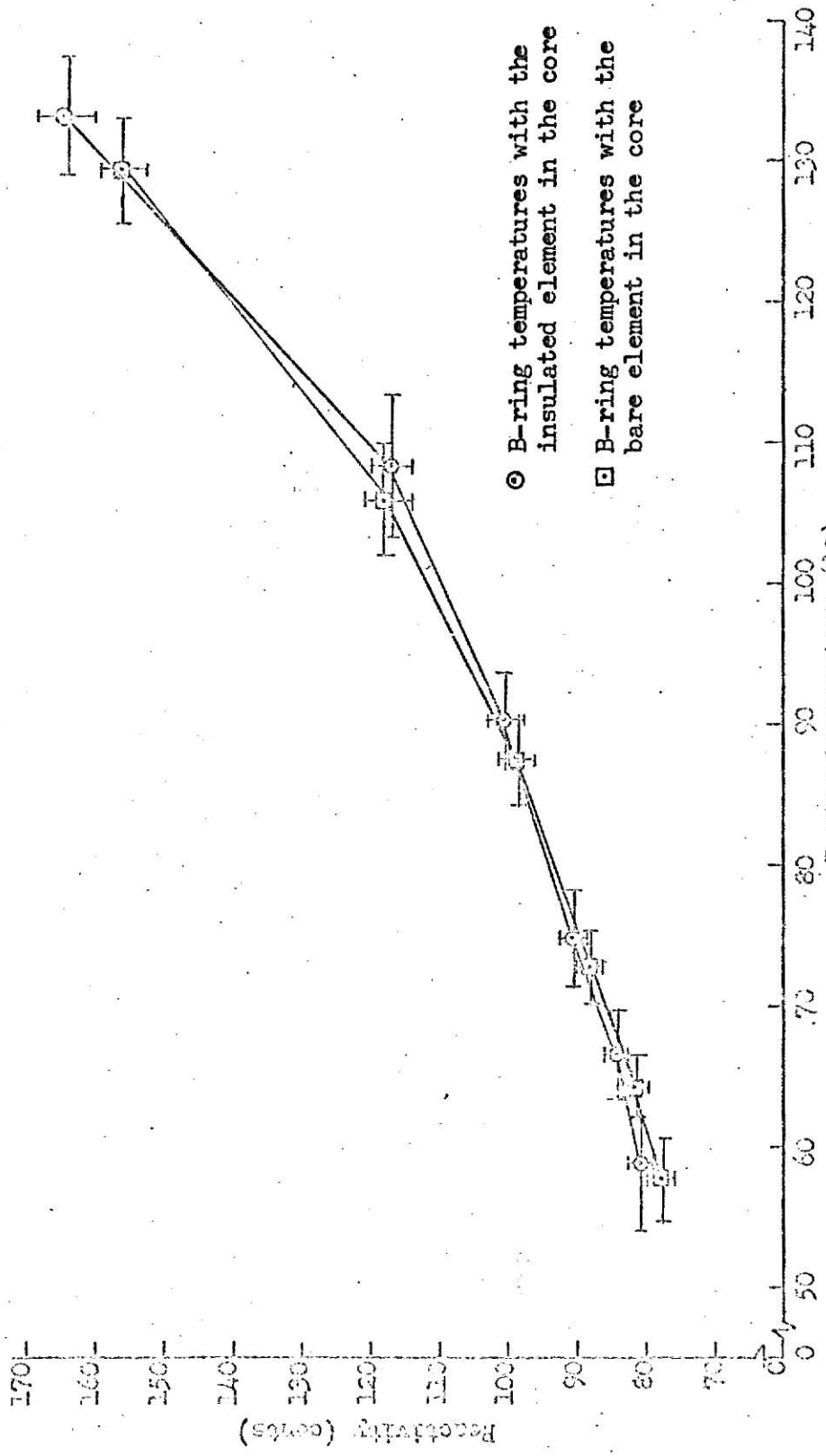

Figure 19. The change in the worth from criticality at 90 kW of the control rods plotted versus the average B-ring temperatures of the twenty runs of both the bare and insulated cases.

where ϕ_o = initial flux

λ = one group decay constant

and the α's are the solutions of

$$\rho = \frac{\alpha}{1 + r'\alpha}\left(r' + \frac{\beta'}{\alpha + \lambda}\right) \tag{53}$$

where ρ = reactivity in units of k/k

r' = prompt neutron lifetime

β' = one group delay fraction

The first term of Eqn. (52) is the stable term and the second is the transient one. The second term goes to zero very fast since α_2 is very large compared to α_1 (4, 6, 7). With this knowledge, Eqn. (52) reduces to

$$\phi(t) = \frac{\alpha_1 + \lambda}{\lambda}\,\phi_o\, e^{\alpha_1 t} \tag{54}$$

For the transient power drop from 90 kW to 10 kW, this reduces to

$$\frac{1}{9} = \frac{\alpha_1 + \lambda}{\lambda}\, e^{\alpha_1 t} \tag{55}$$

The root of this equation can be found for any time, t, and then the reactivity contribution from the delayed neutrons can be found from Eqn. (53).

Figures 20 and 21 are plots of these three effects for the insulated and bare cases, respectively. The reactivities plotted in these figures are the reactivity differential from zero

power to the steady state control rod reactivity worth at 10 kW. The reactivities are plotted versus B-ring temperatures and the temperature effect of reactivity is found by requiring the temperature and control rod effects to cancel the delayed neutron effect.

The difference of the slopes of the linear portion of the temperature effect plot gives the average temperature coefficient for the B-ring temperature range considered (90°C to 58°C). This coefficient is the contribution from the elevation of the temperature of the one insulated element. The number is found to be -0.0294 ¢/°C. This value falls very close to the temperature coefficients calculated from the steady state data. Since three independently obtained mean values for the temperature coefficient have been calculated, an indication of the accuracy of these values can be found from the standard deviation of the means (29). The mean value is $\alpha_T = -0.0300 \pm 0.0010$ ¢/°C. The accuracy associated with this mean value is about 3.3% while the precisions associated with the steady state values are 71% and 81% and the standard deviation of the transient value given above is nearly 510% of the mean value. This large standard deviation is due about half to the uncertainty in the reactivity data and half to the uncertainty in the temperature data.

The total temperature coefficient of the core also can be found from the steady state and transient data if the average core temperature is known. Stauder (16) has developed a procedure to find the average temperature in the TRIGA core as a function

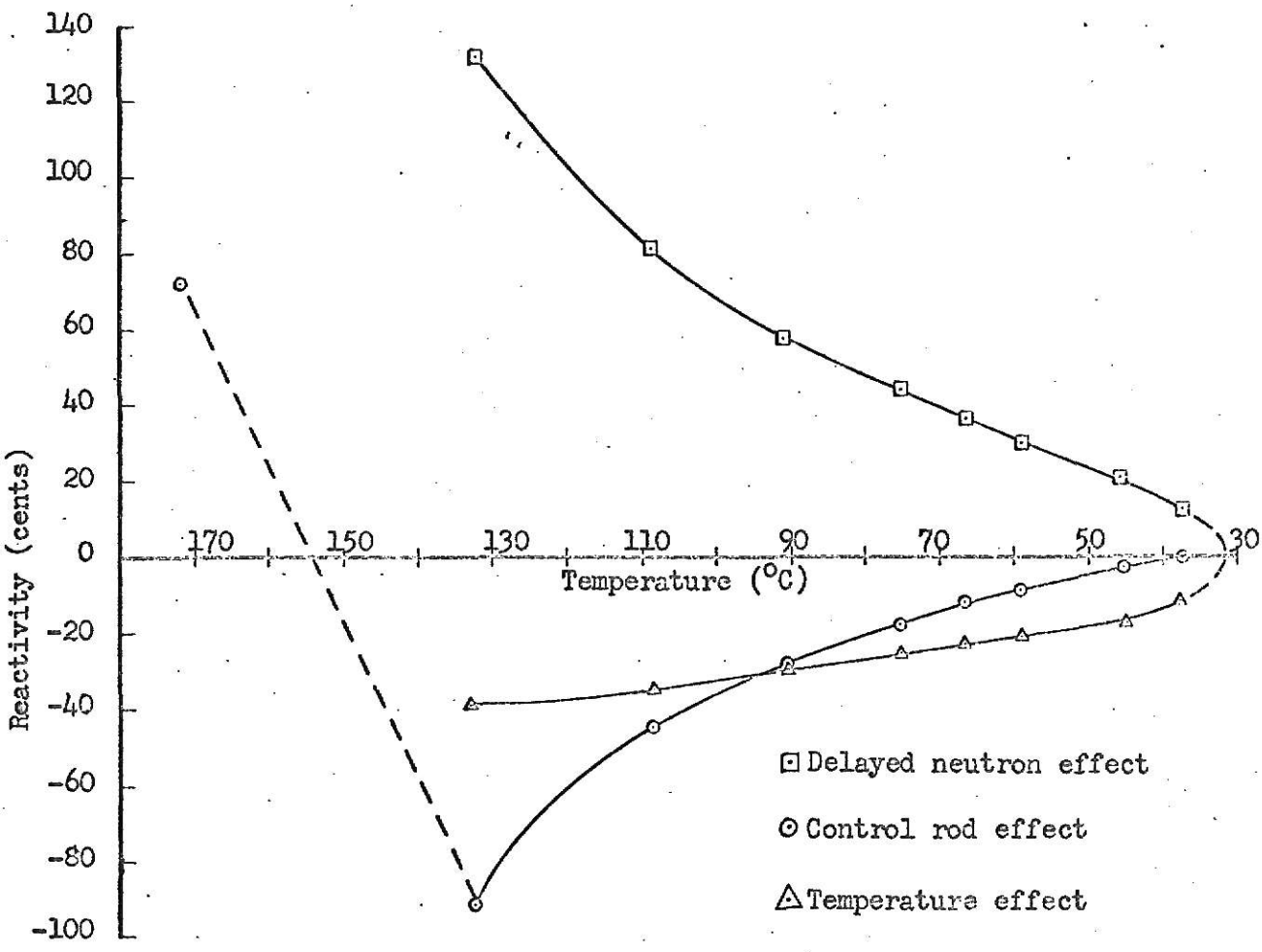

Figure 20. The effect of delayed neutrons, temperature, and control rod movement on reactivity when the insulated element was in the central thimble.

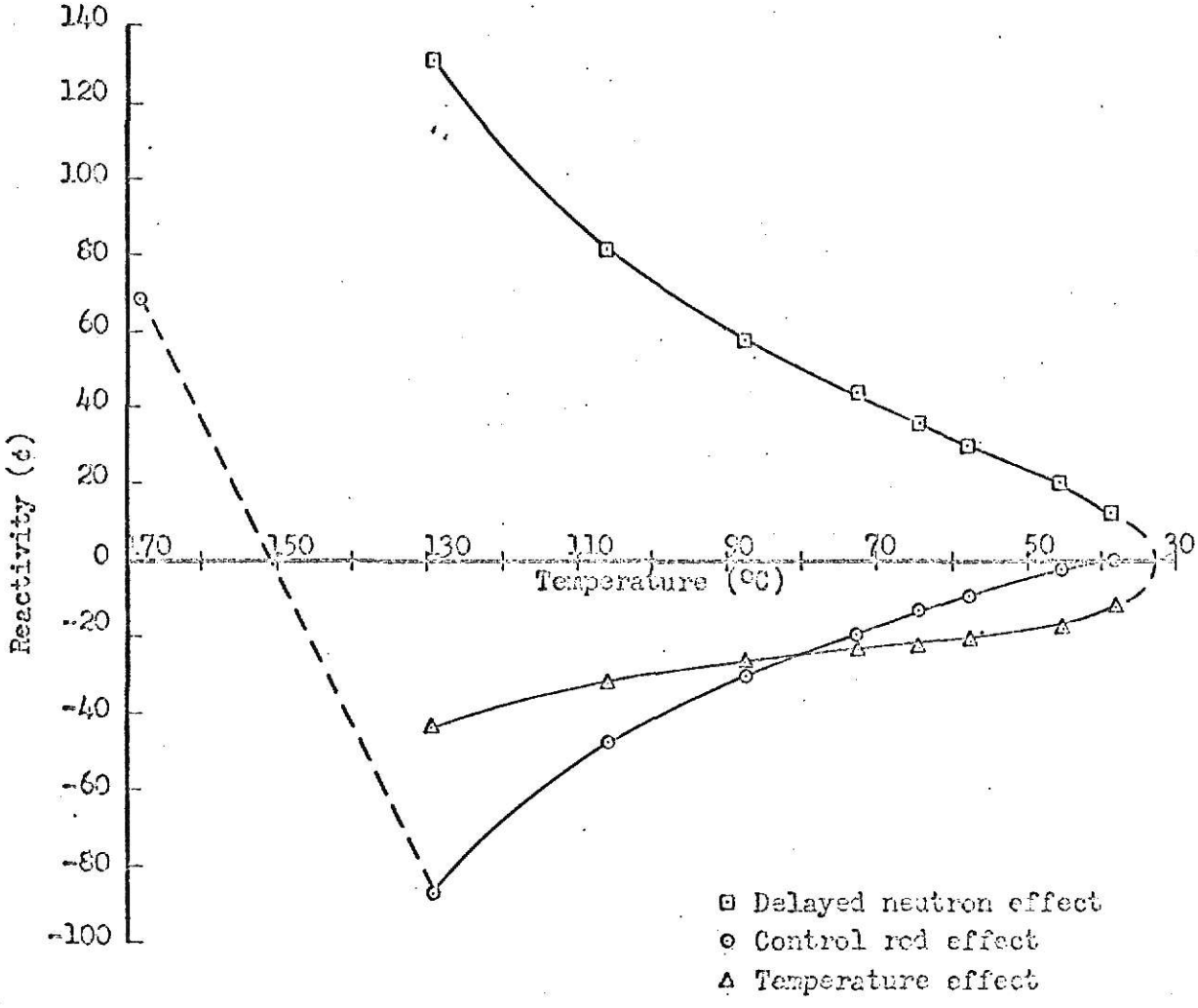

Figure 21. The effect of delayed neutrons, temperature and control rod movement on the reactivity when the bare element was in the central thimble position.

of the reactor power. The average temperature is found from

$$\bar{T} = \frac{\sum_R N_R \bar{T}_R}{\sum_R N_R}$$

where N_R is the number of elements in fuel ring R and $\bar{T}_R$ is the average temperature for a single element in the Rth ring. Using Stauder's data and modifying the average core temperature programs developed by him to handle the new core configuration, average core temperature data were found for both the bare and insulated central thimble fuel element conditions. A plot of these data and the measured B-ring temperature data is shown in Fig. 22. From this figure it is possible to determine the average core temperature knowing the B-ring temperature.

The temperature coefficient for the whole core can be found from the linear portions of the temperature effect curves in Figs. 20 and 21 since now the average fuel temperature of the core can be found. The average core temperature coefficients found from the insulated and bare element transient data are greatly influenced by how accurately the delayed neutron effect curves given in Figs. 20 and 21 reproduce the real effect. The B-ring temperature range over which the single element temperature coefficient was calculated was the range from 58°C to 90°C. The slope of the delayed neutron effect is very nearly constant in this range and because of the differencing method used to find the temperature coefficients this slope has little effect on the value calculated for the central thimble element temperature

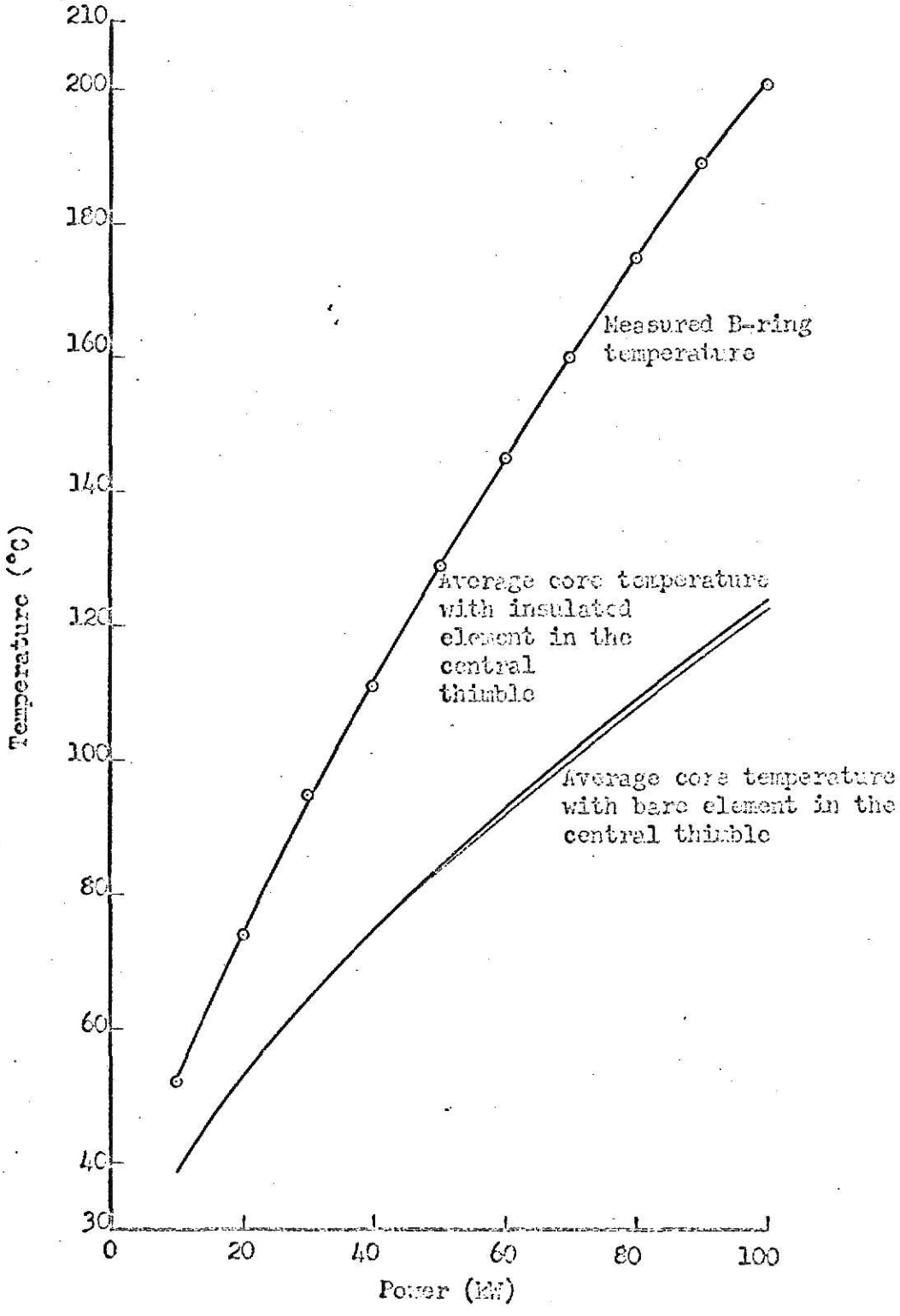

Figure 22. Average core temperature versus power curves for the bare and insulated central thimble element cases. The measured B-ring temperature versus power curve is used as the standard for comparing the bare and insulated data.

coefficient. However, its slope will greatly influence the magnitude of the overall temperature coefficient. The core temperature coefficient found from the insulated element data is -0.468 ± 0.399 ¢/°C and the value for the bare element data is -0.395 ± 0.342 ¢/°C. Stauder reports a value for the temperature coefficient of -0.869 ± 0.020 ¢/°C (temperature range 315°C - 50°C). The method he used to find this coefficient was the same as that employed in the steady state method. Using Fig. 22 to find the average core temperatures for the steady state data, the average temperature coefficient for the core temperature range from 62°C to 42°C found is -1.09 ± 0.80 ¢/°C. This value falls between the value found by Stauder and the coefficient reported in (1) of -1.52 ¢/°C (at 50°C).

The above values cited for the temperature coefficient should be compared with the average theoretical value found earlier in this paper (-1.096 ¢/°C at 215°C). The experimental steady state value and the theoretical value agree and since these numbers lie between the values reported by Stauder and General Atomics, it appears that these numbers are representative of the average temperature coefficient of reactivity of the KSU TRIGA Mark II.

The reason for the discrepancy in the values found from the transient data is due to the analysis of the delayed neutron effect. Since the delayed neutron contribution was only studied analytically, no estimate of the error associated with this effect is known. Therefore, if the slopes of the curves shown in Figs.

20 and 21 were about double that shown in the temperature range of from 58°C to 90°C then the coefficients calculated from the transient data would have magnitudes that fall closer to the other values reported in this thesis.

From the average core temperature data it is also possible to determine an "average" temperature coefficient for any element in the core. The reactivity change caused by the difference in temperature at two power levels may be expressed as

$$\Delta\rho = \sum_R N_R \overline{\Delta T}_R \alpha_{T,R}$$

where $\overline{\Delta T}_R$ is the difference between the two core temperatures for ring R and $\alpha_{T,R}$ is the temperature coefficient for an element in ring R. If the temperature coefficient is assumed independent of temperature then it is the same for all the rings, thus, it may be extracted from the summation. Then, solving for this average temperature coefficient for an element one obtains

$$\alpha_{T,\text{element}} = \frac{\Delta\rho}{\sum_R N_R \overline{\Delta T}_R}$$

The average temperature coefficient per element found in this manner for the insulated case was -0.00726 ¢/°C and for the bare element case it was -0.00633 ¢/°C. In comparing these numbers with the mean value for the temperature coefficient of the element in the central thimble (-0.0301 ¢/°C), one can see the influence of leakage on the temperature coefficient.

Since the coefficient in the center, where the leakage of neutrons is the smallest, is four times as large as the average coefficient; one can account for this by noting that the average coefficients for the outer rings of elements, which are the most subjected to leakage, are greatly influenced by this leakage. This causes the core averaged temperature coefficient per element to be smaller than the central position coefficient and one can assume that the average coefficient per ring decreases for rings of larger and larger radii. This effect may be the reason why the core average temperature coefficient calculated from the steady state data is larger than the value Stauder reported. The changes in the core that the calculations given in this thesis were based on as compared to the core with which Stauder's measurements were taken are that an element was placed in the central thimble and three elements were removed from the F-ring. Therefore, a higher core temperature coefficient was noted because of the effect of leakage influencing an increase in the coefficient due to the central element and the three elements that were removed.

5.0 SUGGESTIONS FOR FURTHER STUDY

The major problem encountered in the experimental investigation was the inability to distinguish with high accuracy the difference between two reactivities of approximately the same magnitude. It is suggested for further study that a fine control rod be constructed so that reactivities that differ by as little as 0.1¢ could be measured. Such a rod could be made to traverse through the core in one of the small flux probe holes in the top grid plate.

Another way to improve this procedure would be to insulate a larger sample so that the reactivity change would be large enough that the precision experienced in this investigation would be adequate enough for the precision needed to obtain small standard deviations in the average changes in reactivity between two power levels. Such a sample would be, for example, all the elements in the B-ring. This would require a number of cold, clean elements and could be performed as part of the check out procedure when the KSU TRIGA core is upgraded with stainless steel fuel elements.

A large number of theoretical experiments should be performed with the code RABBLE now that this code has been made operable on the IBM 360/50 for this investigation. This would make the optimization of future experiments much better. The only drawback is the long running time on this system. The time required for one calculation for the group structure analyzed in this investigation was on the order of 60 minutes.

6.0 ACKNOWLEDGEMENTS

The author wishes to express his gratitude to Dr. M. J. Robinson for his guidance and help throughout this investigation. Special thanks are also extended to Dr. Z. B. Weiss for his help with the neutron thermalization theory presented in this paper. I wish also to thank Mr. R. W. Clack for his help with the experimental procedure and apparatus. Thanks are also extended to the reactor operators; Mr. E. Heckman, Mr. J. McCleskey, and Mr. M. Estes; for their particular contributions to this work. I also wish to thank the National Aeronauties and Space Administration for providing financial support for this investigation by granting the author a NASA Traineeship.

LITERATURE CITED

1. Hazards Summary Report, Engineering Experiment Station Special Report No. 7, Kansas State University, Manhattan, Kansas (1961).

2. Williams, M.M.R.
   The Slowing Down and Thermalization of Neutrons, North-Holland Publishing Co. (1966).

3. Technical Foundation of TRIGA. GA-471 (1958).

4. Lamarsh, J.R.
   Nuclear Reactor Theory, Addison-Wesley (1966).

5. El-Wakil, M. M.
   Nuclear Power Engineering, McGraw Hill (1962)

6. Meghreblian, R.V. and D. K. Holmes
   Reactor Analysis, McGraw-Hill (1960).

7. Glasstone, S. and A. Sesonske
   Nuclear Reactor Engineering, D. Van Nostrand (1963).

8. Fisher, E.A.
   "Interpretation of Doppler Coefficient Measurements in Fast Critical Assemblies," ANL-7320, 350-357 (1966).

9. Storrer, F., et. al.
   "Measurements of the Doppler Coefficient in Large Fast Power Reactors Using a Fast Critical Assembly and an Experimental Fast Reactor," ANL-6796, 823-852 (1963).

10. Till, C. E., et. al.
    "ZPR-6 Doppler Measurements and Comparisons with Theory," ANL-7320, 319-333 (1966).

11. License No. R-88, Technical Specifications for the Kansas State University TRIGA Mark II Reactor.

12. Pucker, N.

"The Measurement of the Doppler Coefficient of Fast Reactors Using Heated Samples," ATKE 12-30, 189-192 (1967).

13. Greebler, P. and E. Goldman

"Measurement of Doppler Coefficient by Heating a Small Region of a Fast Reactor Critical Assembly," Nuclear Science and Engineering, 18, 287-289 (1964).

14. Gasidlo, J. M.

"Results of Recent Doppler Experiments in ZPR-3," ANL-7320, 345-349 (1966).

15. Fischer, G. J., et. al.

"Experimental Results for U-238 Doppler Measurements in Fast Reactor Spectra," ANL-6792, 885-895 (1963).

16. Stauder, J. W.

"An Analysis of the Pulsing Characteristics of the Kansas State University TRIGA Mark II Nuclear Reactor", a Master's Thesis, Kansas State University (1969).

17. Keir, P. H., and A. A. Robba

"RABBLE, A Program for Computation of Resonance Absorption in Multiregion Reactor Cells," ANL-7326 (1967).

18. Strawbridge, L. E. and R. F. Barry

"Criticality Calculations for Uniform Water Moderated

Lattices," Nuclear Science and Engineering, 23, 58-73 (1965).

19. Schmidt, J. J.
"Neutron Cross Sections for Fast Reactor Materials Part I: Evaluation," KFK-120 (1966).

20. Schmidt, J. J.
"Neutron Cross Sections for Fast Reactor Materials Part II: Tables," KFK-120 (1962).

21. McReynolds, A. W., et. al.
"Neutron Thermalization by Chemically Bound Hydrogen and Carbon," Second International Conference on the Peaceful Uses of Atomic Energy, P/1540 (1958).

22. Toppel, B. J. and I. Baksys
"The Argonne-Revised Thermos Code," ANL-7023 (1965).

23. Hughes, D. J. and J. A. Harvey
"Neutron Cross Sections," BNL-325 (1955).

24. Amouyal, A., P. Benoist, and J. Horowitz
"Nouvelle Methode de Determination du Facteur D'Utillisation Thermique D'Une Cellule," Journal of Nuclear Energy, 6, 79-97 (1957).

25. Case, K. M., et. al.
"Introduction to the Theory of Neutron Diffusion," Los Alamos Scientific Laboratory (1953).

26. Stamniler, R. J., S. M. Takac and Z. B. Weiss
"Neutron Thermalization in Reactor Lattice Cells," An NPY Project Report, International Atomic Energy Agency (1966).

27. Bouchey, G. D.

"Experimental Neutron Flux Measurements and Power Calibration in the Kansas State University TRIGA Mark II Nuclear Reactor," A Master's Thesis, Kansas State University (1967).

28. "Thermocouple and Extension Wires," Thermo-Electric Co., Section 332 (1965).

29. Brownlee, K. A.

Statistical Theory and Methodology in Science and Engineering, Wiley & Sons (1965).

APPENDIX A

Temperature Analysis of TRIGA Mark II Insulated Fuel Element

An analysis was performed to determine the expected fuel centerline, fuel surface, and clad surface temperatures as a function of power for an insulated instrumented fuel element in the central thimble of the KSU TRIGA Mark II reactor.

The rate of heat produced per unit volume of the fuel is from El-Wakil (5)

$$q''' = 2.783 \times 10^{-6} N\sigma_f\phi \ \frac{BTU}{hr\ ft^3} \qquad (A.1)$$

N = number of fissionable nuclei/cm^3

σ_f = effective fission cross section of the fuel, cm^2

ϕ = neutron flux

Thus, since N and σ_f are nearly constant the heat generation rate can be said to be proportional to the flux.

$$q''' = K\phi \qquad (A.2)$$

The temperature distribution in solid cylindrical fuel elements can be predicted under the assumption of small axial or radial variation in the flux, heat flow essentially in the radial direction, equal heat flow in all radial directions, and steady state heat transfer. The fuel temperature distribution is given by

$$T_{max} = T_f + q''' R_1^2 \left[\frac{1}{4k_f} + \frac{1}{2R_{cf}R_1} + \frac{1}{2k_c} \ln\left(\frac{R_2}{R_1}\right) + \frac{1}{2hR_2}\right] \qquad (A.3)$$

T_{max} = maximum (centerline) temperature

T_f = bulk fluid temperature

R_1 = radius of the fuel

R_2 = radius of the fuel plus cladding thickness

k_f = thermal conductivity of the fuel

k_c = thermal conductivity of the cladding

h = heat transfer coefficient

R_{cf} = thermal conductance between the cladding and fuel

The thermal conductivities of the fuel and cladding are functions of temperature. Data from reference 3 was used in order to obtain the following equation for the fuel thermal conductivity

$$k_f(T) = 57.78[.17 + .05\, e^{-.00868(\frac{T_{max} + T_{surf}}{2})}] \frac{BTU}{hr\ ft^{\circ}F} \qquad (A.4)$$

T_{max} = maximum fuel temperature, $^{\circ}C$

T_{surf} = fuel surface temperature, $^{\circ}C$

$$T = \frac{T_{max} + T_{surf}}{2}$$

The variation of cladding thermal conductivity was also accounted for in the calculations, but it has only a very slight temperature dependence.

The heat transfer coefficient was found using the Weisman equation as given in El-Wakil

$$Nu = C\ Re^{0.8}\ Pr^{1/3} \qquad (A.5)$$

C = constant which depends on the lattice arrangement

Nu = Nusselt number = $\frac{hD_e}{k_w}$

Re = Reynolds' number = $\frac{D_e V \bar{\rho}}{\mu}$

Pr = Prandtl number

D_e = equivalent diameter of channel

k_w = thermal conductivity of water

V = water velocity

$\bar{\rho}$ = water density

μ = water viscosity

The physical properties are evaluated at the bulk fluid temperature ($70^{\circ}F$). The water velocity in the channel was found by equating the pressure drop due to friction through the core to the hydrostatic pressure change in the core. The equations for the pressure changes are found in El-Wakil. The friction pressure drop is

$$\Delta P_f = f_m \frac{H}{D_e} \frac{\bar{\rho} V^2}{2g_c} \qquad (A.6)$$

f_m = Moody's friction factor

g_c = conversion factor, 32.174 lbm ft/lbf sec^2

H = core height

The hydrostatic pressure drop is

$$\Delta P_h = \bar{\rho} H \frac{g}{g_c} \qquad (A.7)$$

g = gravitational acceleration

Equating Eqns. (A.6) and (A.7) and gives

$$V^2 = \frac{2 D_e g}{f_m} \qquad (A.8)$$

The friction factor is a function of Reynolds' number and channel roughness. Using Moody's friction factor chart for smooth pipes, an iteration was performed until the Reynolds' number calculated using the velocity determined in Eqn. (A.8) was the same as the Reynolds' number at which f was evaluated. Using this velocity, the heat transfer coefficient given by Eqn. (A.5) was determined to be 1640 BTU/hr ft^2 ^oF.

The only unknown left in Eqn. (A.3) is R_{cf}, the thermal conductance of the gap between the cladding and the fuel. Temperature on the fuel element centerline (T_{max}) versus power data were taken using an instrumented fuel element in the B ring of the core. The flux data as a function of power used to calculate q'" were taken from Bouchey (27). R_{cf} was then fit as a function of q'" so that the T_{max} data were reproduced. The R_{cf} thus determined was linear over certain ranges of power and four linear fits of the form

$$R_{cf} = A + Bq''' \qquad (A.9)$$

were used. A and B are constants which depend on the reactor power range.

The thickness of the gap between the fuel and cladding is unknown and R_{cf} physically represents a thermal conductance

across this unknown gap. As q'" increases the fuel and cladding temperatures increase and the fuel and cladding expand causing the gap thickness to decrease. Thus, the increase of R_{cf} with q'" shown in Eqn. (A.9) is comparable with physical expectations. It should be noted that the fit for R_{cf} versus q'" will lead to higher calculated temperatures than will actually occur. This is because R_{cf} is primarily dependent on the fuel expansion against the cladding which is in turn a function of fuel temperature. For the insulated fuel element case, the fuel temperature will be higher for the same q'" as used in the bare case. In essence, then, the contact conductance value used for the insulated case is low and leads to a calculated fuel temperature of a conservative nature (i.e. higher than will actually occur). This approach is taken from the hazards analysis viewpoint.

Based on the above assumptions, a computer program was written to calculate the fuel temperatures as a function of power. For comparison with actual measurements, maximum fuel temperature was calculated for the bare element in the B ring. The same model was then used for predicting the central thimble fuel element temperature values for both the bare and insulated cases.

In the present configuration of the core, the central thimble acts as a "flux trap". With the insertion of a fuel element in the central thimble, the flux will then be depressed. Thus, the values of the central thimble flux taken from Bouchey's data overstate the actual fluxes that will exist for the fueled

central thimble case. The temperatures given in this report therefore represent a conservative estimate of the temperatures that would be reached.

The results of the computer fit are given in Fig. A.1. Temperature versus power curves are shown for the measured and the predicted temperatures in the element in the B ring, for the predicted temperatures for a bare element in the central thimble, and for the temperatures to be reached with 0.008" of Scotchtite insulation on the element in the central thimble. The temperatures for the above conditions are listed in Table A.I as well as the calculated cladding and fuel surface temperatures in the B ring and in the central thimble for the bare and insulated cases. Figure A.2 shows the calculated radial temperature distribution in a fuel element at 100 kW for the B ring and the central thimble bare and insulated cases.

The fuel temperature limitation for the core is 450°C (11). All experimentation must be done such that the maximum temperature reached in the insulated elements will be less than 450°C. According to the above conservative analysis the temperatures reached during experimentation will be below the maximum allowable temperature for powers at least up to 100 kW. The temperature in any configuration was monitored as the power was increased in order to double check the calculations. Due to the conservative nature of the calculations the insulated central thimble element temperature reached only 275°C at 100 kW as compared to the calculated temperature of 410°C.

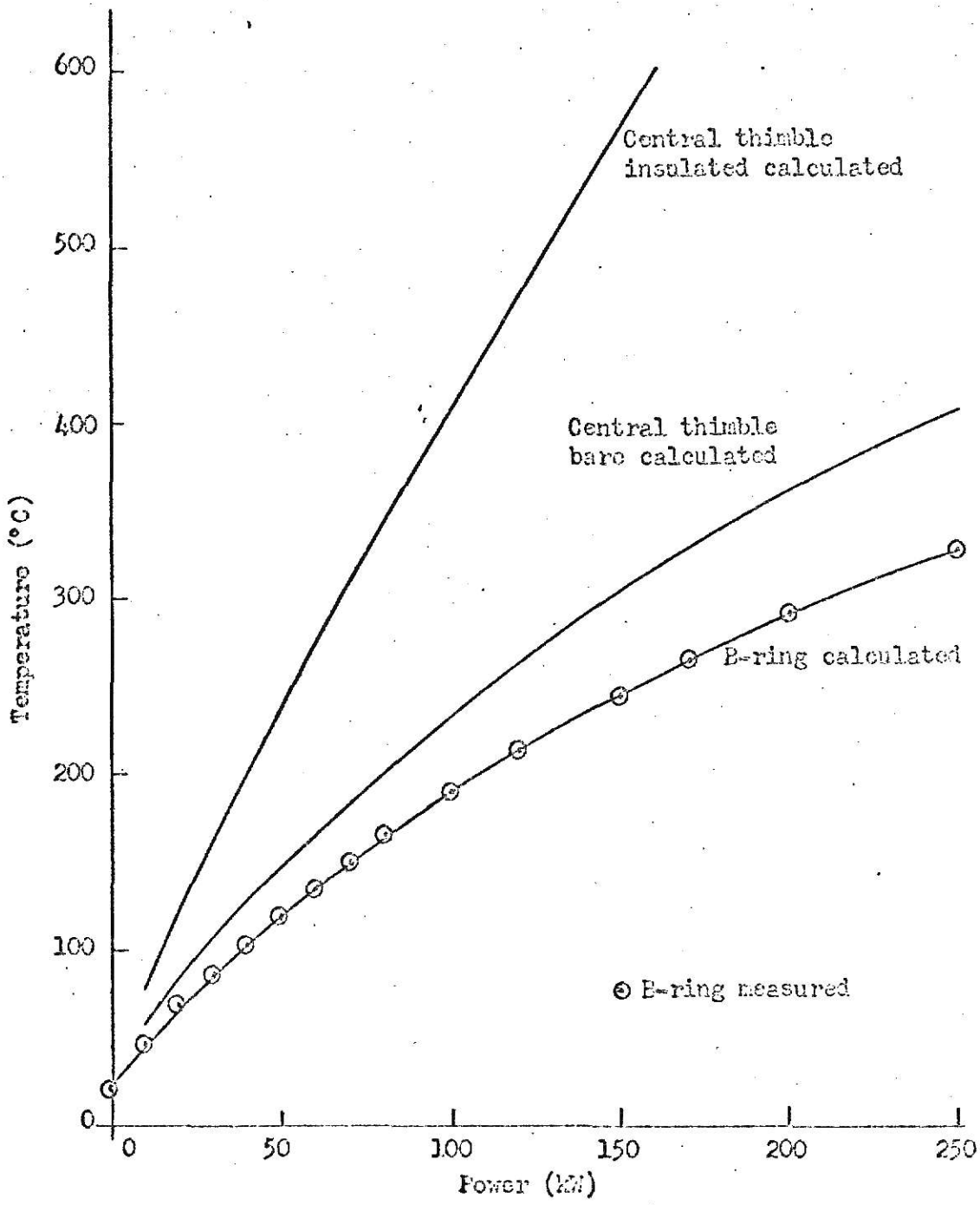

Figure A.1. Temperature versus power plot for KSU TRIGA Mark II Reactor showing the centerline temperatures predicted for an insulated fuel element in the central thimble position.

TABLE A.I

TEMPERATURE ANALYSIS OF INSULATED FUEL ELEMENT
IN CENTRAL THIMBLE OF TRIGA MARK II REACTOR

REACTOR POWER (KW)	TMAX FUEL DEG C			TSURF FUEL DEG C			TSURF CLAD DEG C		
	BRINGM	BRINGC	CTBARE	CTINS	BRINGC	CTBARE	CTINS	BRINGC	CTBARE	CTINS
10	46.0	46.3	56.1	73.6	42.2	50.1	67.4	22.1	22.5	39.9
20	67.0	67.2	83.3	118.5	58.8	71.9	105.6	23.0	23.9	58.6
30	85.0	85.2	105.8	158.7	72.2	86.8	138.8	24.0	25.3	77.3
40	101.0	100.9	125.1	195.7	83.4	99.3	168.7	24.9	26.7	96.1
50	118.0	117.5	146.0	234.3	95.4	113.3	200.1	25.9	28.1	114.8
60	134.0	133.2	165.5	271.5	106.2	125.9	230.0	26.8	29.5	133.6
70	149.0	148.0	183.9	307.6	116.2	137.2	258.7	27.8	30.8	152.3
80	165.0	162.0	201.3	342.6	125.5	147.6	286.4	28.7	32.2	171.1
100	189.0	188.2	233.8	410.0	141.9	165.7	339.2	30.6	35.0	208.6
120	213.0	212.4	263.7	474.8	156.3	181.3	389.4	32.5	37.8	246.0
150	245.0	245.6	305.0	568.2	174.7	201.0	461.2	35.4	42.0	302.3
170	266.0	266.4	330.1	628.1	185.5	211.7	506.6	37.3	44.8	339.8
200	292.0	292.4	363.0	713.0	196.6	223.0	569.9	40.2	48.9	396.0
250	328.0	327.5	409.3	846.0	207.0	233.4	667.0	44.9	55.9	489.7

BRINGM = B ring measured BRINGC = B ring calculated
CTBARE = Central thimble bare CTINS = Central thimble insulated

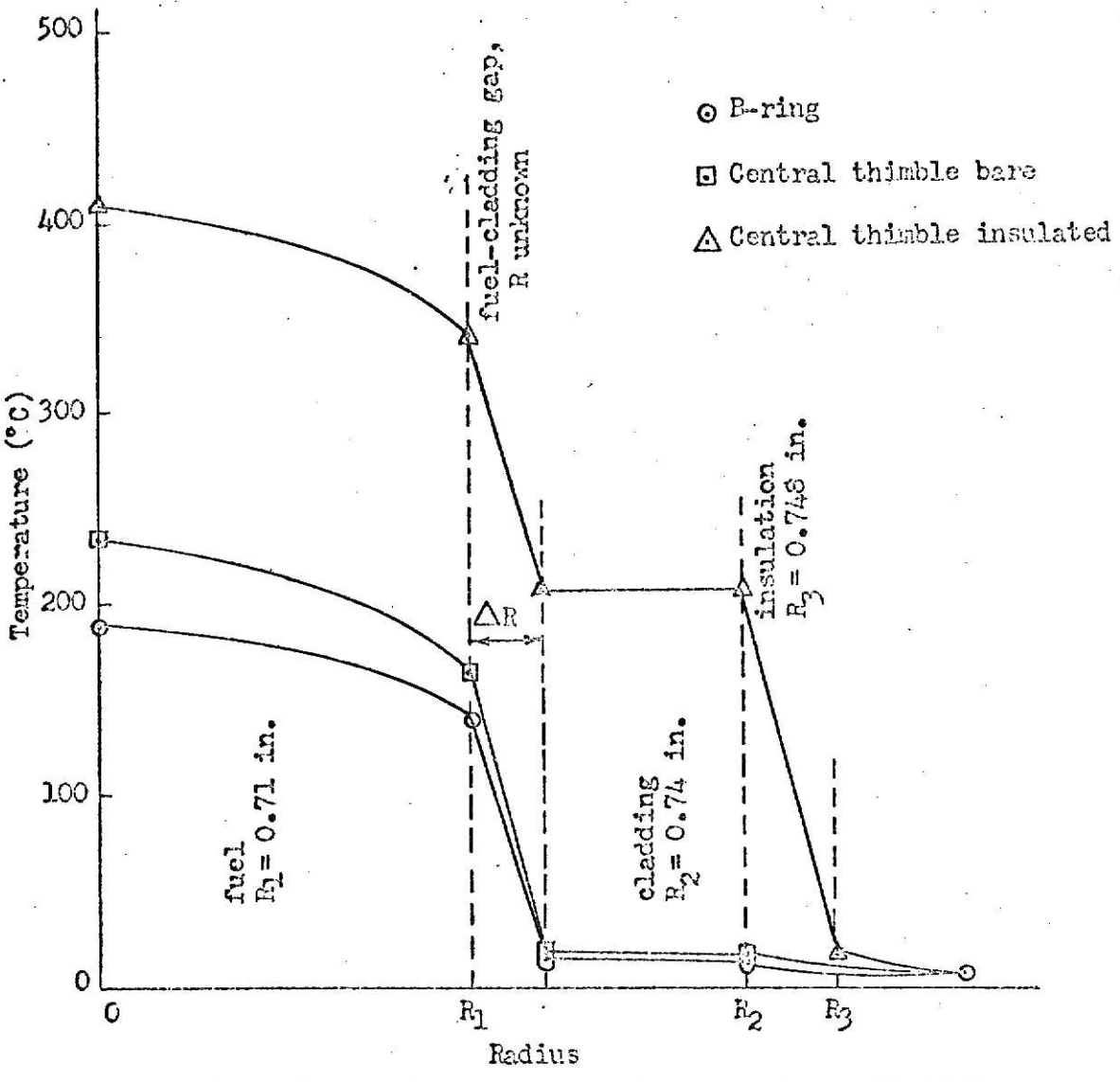

Figure A.2. Temperature versus radius plot for a KSU TRIGA Mark II Reactor fuel element at 100 kW.

APPENDIX B

ZIRK, A Scattering Kernel Code for Zirconium Hydride

B.1 Introduction

The computer code ZIRK follows the same calculational procedure as does GAKER (22). The only major change from GAKER is that the scattering kernel as given by McReynolds for ZrH is substituted for the water kernel.

The typical running time on the IBM 360/50 is about 10 minutes for a 30 group calculation of the scattering kernel and group scattering cross sections.

Some of the variables used in the program are defined in the FORTRAN listing and others are defined in the input data given below.

B.2 Main Program Input Data Format

Card 1: FORMAT(I5,E15.8)

NE - number of energy groups

T - temperature of the medium (^{o}K)

Cards 2-7: FORMAT(5E15.8)

E(I) - energy of group I (eV)

B.3 ZIRK Output Data Format

Cards 1-6: FORMAT(5E15.8)

SO(I) - scattering cross section in barns for group I

Cards 7-156: FORMAT(6E13.6)

PO(J,I) - the scattering kernel from group I to group J

Figure B.1 shows the scattering cross section output of ZIRK for temperatures of 293°K and 773°K. This figure shows how the characteristic "wiggles" in the cross section, that were noted experimentally by McReynolds (21), are smoothed out with increasing temperature in the medium.

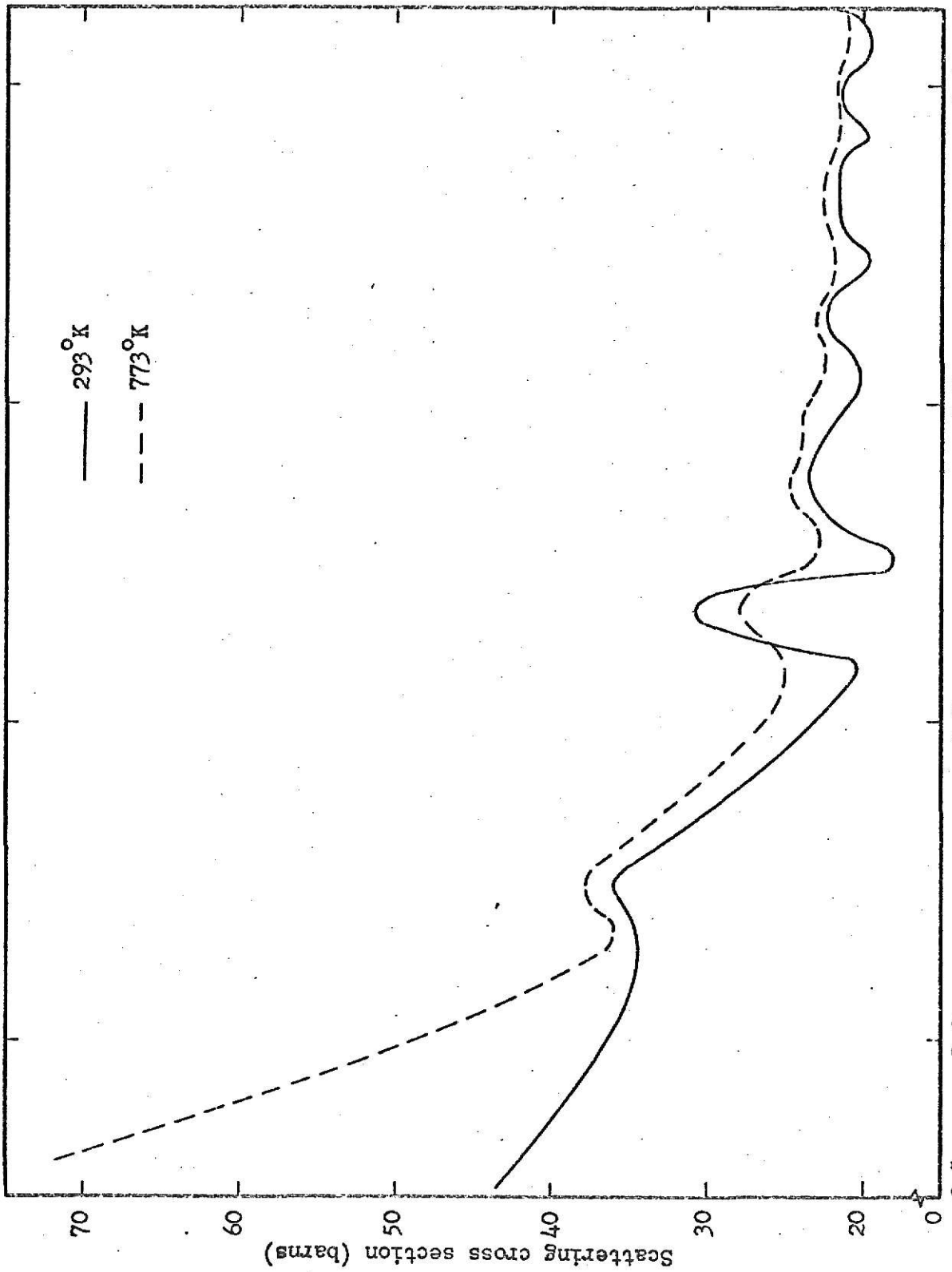

Figure B.1. A plot showing the effect of temperature on the scattering cross section of hydrogen in zirconium hydride.

B.4 FORTRAN Listing of ZIRK

```
      DIMENSION P0(55,55),S0(55,55),TRX(55),V(55),WV(55),E(55)
11    FORMAT(I5,E15.8)
12    FORMAT(5E15.8)
1     READ(1,11) NE,T
      IF(T.EQ.0.0) CALL EXIT
      READ(1,12)(E(I),I=1,NE)
C   CALCULATION OF THE VELOCITIES FROM THE ENERGIES
      DO 9 I=1,NE
9     V(I)=SQRT(E(I)/0.0253)
C   WV(I) IS THE VELOCITY INTERVAL AROUND V(I)
      WV(1)=2.*V(1)
      WV(2)=2.*(V(2)-WV(1))
      DO 3 I=3,NE
3     WV(I)=2.*(V(I)-(V(I-1)+WV(I-1)/2.))
      WRITE(3,15) (I,V(I),I=1,NE)
      WRITE(3,16) (I,WV(I),I=1,NE)
   15 FORMAT(/,'  I  V(I)',/,(7(I3,E12.4)))
   16 FORMAT(/,'  I  DV(I)',/(7(I3,E12.4)))
      CALL ZIRK(NE,T,P0,S0,TRX,V,WV,E)
      GO TO 1
2     STOP
      END
      SUBROUTINE ZIRK(NE,T,P0,S0,TRX,V,WV,E)
      DIMENSION V(55),E(55),P0(55,55),P1(55,55),ANG(30),BF(30),W(30),
     1          S0(55),S1(55),TRX(55),P(55,55),WV(55),U(55)
      DATA ANG(1),ANG(2),ANG(3),ANG(4),ANG(5),ANG(6),ANG(7),ANG(8),
     1ANG(9),ANG(10),ANG(11),ANG(12),ANG(13),ANG(14),ANG(15)
     2/-.98799,-.93727,-.84821,-.72441,-.57097,-.39415,-.20199,0.0,
     3.20119,.39415,.57097,.72441,.84821,.93727,.98799/
      DATA W(1),W(2),W(3),W(4),W(5),W(6),W(7),W(8),W(9),W(10),W(11),
     1W(12),W(13),W(14),W(15)/.01537,.03518,.05358,.06978,.08314,
     2.09308,.09921,.10129,.09921,.09038,.08314,.06978,.05358,.03518,
     3.01537/
      NLARG=9
      NA=15
      DO 35 I=1,NE
      DO 35 J=1,NE
      P0(I,J)=0.0
      P1(I,J)=0.
   35 CONTINUE
C   DATA FOR THE ZIRCONIUM HYDRIDE KERNEL
      T=(T*8.61706E-05)/0.0253
      W0=0.13
      BARNS=81.6
      PI=3.141593
      OMEGA=W0/0.0253
      B=(OMEGA*SINH(OMEGA/(2.*T)))
      A=(OMEGA*TANH(OMEGA/(2.*T)))
      XLAM=1.0/91.0
      DO 170 K=1,NA
C   THE K DO LOOP PERFORMS THE INTEGRATION OVER THE ANGLES USING
C   15-POINT GAUSSIAN QUADRATURE
      DO 170 I=1,NE
      DO 170 J=I,NE
C   THE I & J DO LOOPS ARE USED TO CALCULATE THE UPPER TRIANGULAR
C   PORTION OF THE SCATTERING KERNEL P0(I,J)
      VI=V(I)
      VJ=V(J)
```

```
      NDG=0
      IF(I.NE.J) GO TO 1045
      VI=VJ-.625*WV(J)
      STOR=0.
 1040 NDG=NDG+1
      VI=VI+.25*WV(J)
 1045 EI=VI*VI
      EJ=VJ*VJ
      Z=EI+EJ-2.*ANG(K)*VI*VJ
   38 SUM2=0.
      FRONT=SQRT(EI/EJ)*SQRT(1.0/(4.*PI*XLAM*T*Z))*EXP(-Z/A)
      ZP=Z/8
      CALL BESLIN(ZP,NLARG,BF)
C     THIS DO LOOP PERFORMS THE SUMMATION OVER N FROM -INFINITY TO
C     +INFINITY WHERE TERMS OUTSIDE THE RANGE FROM -8 TO +8 DO NOT
C     CONTRIBUTE TO THE SUMMATION
      DO 90 N=1,17
      NP=N-9
      NPA=1+IABS(NP)
      XNP=NP
      ARG1=XNP*OMEGA/(2.*T)
      ARG2=((EI-EJ+XNP*OMEGA+XLAM*Z)**2)/(4.*T*XLAM*Z)
      ARG=ARG2-ARG1
      IF(ARG.GT.40.) GO TO 81
      TERMA=EXP(-ARG)
      GO TO 82
81    TERMA=0.0
82    DUM=TERMA*BF(NPA)*FRONT
      SUM2=SUM2+DUM
90    CONTINUE
      IF(NDG.LE.0) GO TO 165
      STOR=STOR+SUM2
      IF(NDG.LT.4) GO TO 1040
      SUM2=.25*STOR
  165 P0(I,J)=P0(I,J)+W(K)*SUM2
      P1(I,J)=P1(I,J)+W(K)*SUM2*ANG(K)
  170 CONTINUE
C     THE FOLLOWING DO LOOP CONVERTS THE KERNEL FROM ENERGY SPACE TO
C     VELOCITY SPACE
      DO 180 I=1,NE
      DO 180 J=I,NE
      FACT=2.*BARNS*V(I)*V(J)
      P0(I,J)=FACT*P0(I,J)
      P1(I,J)=FACT*P1(I,J)
  180 CONTINUE
      NEP=NE-1
C     THE FOLLOWING DO LOOP USES THE DETAILED BALANCE CONDITION TO
C     CALCULATE P0(J,I) FROM P0(I,J)
      DO 190 I=1,NEP
      M=I+1
      DO 190 J=M,NE
      FACT=E(J)/E(I)*EXP((E(I)-E(J))/T)
      P0(J,I)=FACT*P0(I,J)
      P1(J,I)=FACT*P1(I,J)
  190 CONTINUE
C     S0(I) IS THE SCATTERING CROSS SECTION
C     TRX(I) IS THE TRANSPORT CROSS SECTION
      DO 202 I=1,NE
      S0(I)=0.
      S1(I)=0.
```

```
      DO 200 J=1,NE
      S0(I)=S0(I)+P0(J,I)*WV(J)
      S1(I)=S1(I)+P1(J,I)*WV(J)
  200 CONTINUE
      VINV=1./V(I)
      S0(I)=S0(I)*VINV
      S1(I)=VINV*S1(I)
      U(I)=S1(I)
      TRX(I)=S0(I)-S1(I)
  202 CONTINUE
 2001 FORMAT(5E15.8)
      WRITE(2,2001)(S0(I),I=1,NE)
      WRITE(3,230) (I,S0(I),I=1,NE)
      WRITE(3,250) (I,TRX(I),I=1,NE)
  230 FORMAT(/' SCATTERING CROSS SECTION, ZERO TH LEGENDRE COMPONENT',
     1       (7(I3,E12.4)))
  240 FORMAT(6E13.6)
  250 FORMAT(/,' TRANSPORT CROSS SECTION',/,(7(I3,E12.4)))
      DO 195 I=1, NE
      VI=1./V(I)
      DO 195 J=1,NE
      P0(I,J)=P0(I,J)*WV(J)*VI
  195 CONTINUE
 2000 FORMAT(6E13.6)
      WRITE(2,2000)((P0(J,I),J=1,NE),I=1,NE)
      WRITE(3,210) ((I,J,P0(J,I),J=1,NE),I=1,NE)
  210 FORMAT(' SCATTERING KERNEL - ZEROTH LEGENDRE COMPONENT  I   J  P
     1I,J)'//,(5(2I4,E12.4)))
      RETURN
      END
      SUBROUTINE BESLIN(X,NMAX,BF)
C CALCULATION OF BESSEL FUNCTIONS I(N) FOR ARGUMENT X FROM I(NMAX-1) D
C TO I(0), THEY ARE CALLED BF(N),,,,,,BF(1), NMAX MAY NOT EXCEED 20.
      DIMENSION BF(30)
      X=ABS(X)
      IF(X.GT.2.0E-05) GO TO 2
      BF(1)=1.0
      A=0.5*X
      DO 1 N=2,NMAX
1     BF(N)=A*BF(N-1)/FLOAT(N-1)
      RETURN
2     A=1.0/X
      BF(15)=0.0
      BF(14)=1.0E-37
      SUM=2.0E-37
      N=14
3     IF(N.EQ.1) GO TO 4
      N=N-1
      BF(N)=2.0*FLOAT(N)*A*BF(N+1)+BF(N+2)
      SUM=2.0*BF(N)+SUM
      GO TO 3
4     A=EXP(X)/(SUM-BF(1))
      DO 5 N=1,NMAX
5     BF(N)=A*BF(N)
      RETURN
      END
```

APPENDIX C

GROUPS, A Program to Homogenize the TRIGA Cell

C.1 Introduction

This computer program was written to perform a homogenization of the cell in the TRIGA reactor. The procedure used is basically that outlined by Strawbridge (18). The calculations for a given temperature of the fuel can be performed in less than three minutes on the IBM 360/50.

The input and output parameters are described below and some of the logic is described in the FORTRAN listing

C.2 Input Data Format

Cards 1-126: FORMAT(5E15.8)

TABLE(I,J,K) - the table of cross sections; I refers to the element, J refers to the type, and K refers to the energy group

Cards 127-133: FORMAT(5E15.8)

DEN(I,J) - neutron density of element I in region J where J refers to as follows: 1=fuel, 2=clad, & 3=moderator

Cards 134-139: FORMAT(5E15.8)

E(K) - energy of group K (eV)

Cards 140-141: FORMAT(5E15.8)

R(I) - radius of region I (same as J described above)

VOL(I) - volume fraction of region I (same as J described above)

Cards 142-143: FORMAT(5E15.8)

AMU(J) - mass number of element J (same as I described above)

Cards 144-293: FORMAT(6E13.6)

P(I,J) - scattering kernel from ZIRK for the temperature of the fuel

Cards 294-443: FORMAT(6E13.6)

Q(I,J) - scattering kernel for water from GAKER at 293°K

C.3 Output Data Format

Cards 1-150 FORMAT(6E13.6)

SIGS(I,J) - homogenized scattering kernel

Cards 151-156: FORMAT(5E15.8)

HOMOAB(K) - homogenized absorption cross section for group K

Cards 157-162: FORMAT(5E15.8)

HOMOSC(K) - homogenized scattering cross section for group K

Cards 163-168: FORMAT(5E15.8)

HOMOF(K) - homogenized fission cross section for group K

C.4 FORTRAN Listing of GROUPS

```
      DIMENSION TABLE(7,3,30),TERM1(30),TERM2(30),TERM3(30),CLADDA(30
     1HOMOF(30),DEN(7,3),E(30),V(30),VOL(3),R(3),FUELAB(30),FUELSC(30
     2CLADAB(30),CLADSC(30),HOMOAB(30),HOMOSC(30),P(30,30),Q(30,30),
     3FUELDA(30),SIGS(30,30),WV(30),AMU(7),SIGH(7)
      REAL MODDA(30),MODAB(30),MODSC(30)
      REAL I0,I1,K0,K1
C     TABLE(I,J,K) IS THE TABLE OF MICROSCOPIC CROSS SECTIONS
C     K REFERS TO THE ENERGY GROUP
C     J REFERS TO TYPE; 1=ABSORPTION, 2=SCATTERING, & 3=FISSION
C     I REFERS TO THE ELEMENT; 1=H(ZRH), 2=C, 3=AL, 4=ZR, 5=U235,
C     6=U238, & 7=H(H2O)
      DO 10 I=1,7
      DO 10 J=1,3
10    READ(1,100)(TABLE(I,J,K),K=1,30)
100   FORMAT(5E15.8)
300   FORMAT(7E15.8)
      DO 110 I=1,7
110   READ(1,100) (DEN(I,J),J=1,3)
      READ(1,100)(E(K),K=1,30)
      READ(1,100)(R(I),VOL(I),I=1,3)
      READ(1,100)(AMU(J),J=1,7)
      DO 20 K=1,30
      V(K)=SQRT(E(K)/0.0253)
      TABLE(3,1,K)=0.23/V(K)
20    TABLE(4,1,K)=0.18/V(K)
      WV(1)=2.0*V(1)
      WV(2)=2.0*(V(2)-WV(1))
      DO 9 I=3,30
9     WV(I)=2.0*(V(I)-(V(I-1)+WV(I-1)/2.))
      DO 400 I=1,7
      IF(AMU(I).LT.1.1) GO TO 401
      ALP=((AMU(I)-1.)/(AMU(I)+1.))**2
      SIGH(I)=1.+ALP*ALOG(ALP)/(1.-ALP)
      GO TO 400
401   SIGH(I)=1.0
400   CONTINUE
      T2=0.076
      XNUBAR=4.0/565.0
      D2=0.333333/(1.2*DEN(3,2))
C     IN THE FOLLOWING DO LOOP THE MACROSCOPIC CROSS SECTIONS AND THE
C     DISADVANTAGE FACTORS ARE CALCULATED FOR EACH GROUP K
      DO 30 K=1,30
      SUM=0.0
      VUM=0.0
      ASORC=0.0
      DO 40 I=1,7
      VUM=VUM+DEN(I,1)*TABLE(I,2,K)
      ASORC=ASORC+DEN(I,1)*TABLE(I,2,K)*SIGH(I)
40    SUM=SUM+DEN(I,1)*TABLE(I,1,K)
      ASORC=ASORC*VOL(1)
      FUELAB(K)=SUM
      FUELSC(K)=VUM
      CLADAB(K)=TABLE(3,1,K)*DEN(3,2)
      CLADSC(K)=TABLE(3,2,K)*DEN(3,2)
      CAPASQ=CLADAB(K)/D2
      TERM1(K)=CAPASQ*T2*T2*FUELAB(K)/CLADAB(K)
      STARSF=FUELSC(K)*(1.-XNUBAR)
      START=STARSF+FUELAB(K)
```

```
      ARG=START*R(1)
      PC=(2.*ARG+1.0/((1.0+ARG/2.29)**4.58)-1.0)/(2.*ARG)
      IF(ARG.GE.0.5) GO TO 50
      ALPHA=0.0331*ARG/0.5
      BETA=0.0186*ARG/0.5
      GO TO 51
50    ALPHA=-.4133333E-02+.8122593E-01*ARG-.1453651E-01*ARG**2+
     1.1451852E-02*ARG**3
      BETA=-.149498CE-01+.1168386*ARG-.1345515*ARG**2+.8290985E-01*ARG
     13-.2754048E-01*ARG**4+.3948718E-02*ARG**5+.1521647E-03*ARG**6
     2-.1075336E-03*ARG**7+.8571787E-05*ARG**8
51    CONTINUE
      TERM2(K)=1.0+(FUELAB(K)/START)*(PC/(1.0-PC)-ARG)*(1.0+ALPHA
     1*STARSF/START +BETA*(STARSF/START)**2)
      CLADDA(K)=TERM2(K)+TERM1(K)/2.0
      TUM=0.0
      DUM=0.0
      BSORC=0.0
      DO 60 I=1,7
      DUM=DUM+DEN(I,3)*TABLE(I,1,K)
      BSORC=BSORC+DEN(I,3)*TABLE(I,2,K)*SIGF(I)
60    TUM=TUM+DEN(I,3)*TABLE(I,2,K)
      BSORC=BSORC*VEL(3)
      MODSC(K)=TUM
      MODAB(K)=DUM
      D3=0.333333/TUM
      CAPMOD=SQRT(MODAB(K)/D3)
      X=CAPMOD*R(2)
      CALL BESSEL(I0,I1,K0,K1,X)
      A=I0
      B=I1
      C=K0
      D=K1
      X=CAPMOD*R(3)
      CALL BESSEL(I0,I1,K0,K1,X)
      TERM=(I1*C+A*K1)/(I1*C-B*K1)
      BIGX=(0.5*CAPMOD*(R(3)**2-R(2)**2)/R(2))*TERM-1.0
      TRANS=DUM+TUM-TUM/27.
      ARG=TRANS*R(2)
      IF(ARG.GT.1.0) GO TO 70
      XLAMBA=0.2442/(ARG+0.4316)+0.7675
      GO TO 71
70    XLAMBA=0.2920/(ARG+0.28)+0.7104
71    CONTINUE
      SERM=(2.*BIGX)/(3.*DUM*(R(3)**2-R(2)**2))+(XLAMBA-2./3.)/R(2)
      TERM3(K)=(1.5*R(1)**2*SUM*(1.+((VEL(2)*CLADAB(K))/(VEL(1)*SUM))
     1*CLADDA(K)))*SERM
      RATIO=FUELAB(K)*VEL(1)/(MODAB(K)*VEL(3))
      TERMA=TERM1(K)+TERM2(K)+TERM3(K)
      TERMB=1.0+TERM1(K)+(TERM2(K)-1.)/RATIO+TERM3(K)/RATIO
      FM=1.0/(1.0+RATIO*TERMB)
      FF=1.0/(1.0+TERMA/RATIO)
      MODDA(K) =RATIO*((ASORC*FM+BSORC*(1.-FF))/(ASORC*(1.-FM)+
     1BSORC*FF))
30    CONTINUE
C     PRINT OUT THE CROSS SECTIONS FOR EACH REGION
      WRITE(3,103)
      DO 90 K=1,30
90    WRITE(3,104) K,FUELAB(K),FUELSC(K),CLADAB(K),CLADSC(K),MODAB(K),
     1MODSC(K)
```

```
104   FORMAT(5X,I5,6(5X,E13.6))
103   FORMAT(1H1,47X,'GROUP CROSS SECTION DATA'/,'      GROUP        FL
     1ABS          FUEL/SCAT          CLAD/ABS          CLAD/SCAT
     2  MOD/ABS          MOD/SCAT')
C    CALCULATE THE AVERAGE FLUXES IN EACH GROUP FROM THE DISADVANTAGE
C    FACTORS THEN PRINT THEM OUT
      DO 220 K=1,30
      FUELDA(K)=1.0/(VOL(1)+VOL(2)*CLADDA(K)+VOL(3)*MODDA(K))
      CLADDA(K)=CLADDA(K)*FUELDA(K)
220   MODDA(K)=MODDA(K)  *FUELDA(K)
      WRITE(3,101)
101   FORMAT('1      DISADVANTAGE FACTORS'/,'      GROUP          CLAD
     1  MODERATOR          FUEL')
102   FORMAT(5X,I5,3(5X,F10.7))
      DO 80 K=1,30
80    WRITE(3,102) K,CLADDA(K),MODDA(K),FUELDA(K)
2000  FORMAT(6E13.6)
2001  FORMAT(5E15.8)
      READ(1,2000)((P(I,J),J=1,30),I=1,30)
      READ(1,2000)((Q(I,J),J=1,30),I=1,30)
C    THE MACROSCOPIC SCATTERING KERNEL IS CALCULATED WITH THE PROPER
C    FLUX AND VOLUME WEIGHTING FROM THE TWO SCATTERING KERNELS IN
C    ZRH (P(I,J)) AND WATER (Q(I,J)) WITH THE INCLUSION OF THE NON
C    MODERATING ELEMENTS CONTRIBUTIONS TO THE SCATTERING ON THE
C    DIAGONAL OF THE NEW KERNEL SIGS(I,J)
      DO 230 I=1,30
      DO 230 J=1,30
      DIAG=0.0
      IF(I.EQ.J) GO TO 231
      GO TO 232
231   DIAG=V(I)*((FUELSC(I)-DEN(1,1)*TABLE(1,2,I))*VOL(1)*FUELDA(I)+
     1VOL(2)*CLADDA(I)*CLADSC(I)+(MODSC(I)-DEN(7,3)*TABLE(7,2,I))
     2*VOL(3)*MODDA(I))*WV(I)
232   SIGS(I,J)=(P(I,J)*DEN(1,1))*VOL(1)*FUELDA(I)+(Q(I,J)*DEN(7,3))*
     1(3)*MODDA(I)+DIAG
230   CONTINUE
C    PRINT OUT THE SCATTERING KERNEL
      WRITE(3,106)((I,J,SIGS(I,J),I=1,30),J=1,30)
106   FORMAT('1      SCATTERING KERNEL  I  J  SIGS(I,J)'//,(6(2I4,E12.
     1))
C    CALCULATION OF THE HOMOGENIZED SCATTERING CROSS SECTIONS FROM THE
C    NEW KERNEL
      DO 240 I=1,30
      SUM=0.0
      DO 250 J=1,30
250   SUM=SUM+SIGS(I,J)*WV(J)*V(J)
240   HOMOSC(I)=SUM/(V(I)*WV(I))
      WRITE(3,105)
105   FORMAT('1          HOMOGENIZED CROSS SECTIONS'/,'      GROUP
     1ABSORPTION        SCATTERING          FISSION'/)
C    CALCULATION OF THE HOMOGENIZED ABSORPTION AND FISSION CROSS
C    SECTIONS BY WEIGHTING THE CROSS SECTIONS WITH VOLUME FRACTIONS
C    AND AVERAGE FLUXES
      DO 200 K=1,30
      HOMOAB(K)=VOL(1)*FUELAB(K)*FUELDA(K)+VOL(2)*CLADAB(K)*CLADDA(K)
     1VOL(3)*MODAB(K)*MODDA(K)
      HOMOF(K)=VOL(1)*TABLE(5,3,K)*FUELDA(K)*DEN(5,1)
200   WRITE(3,104)K,HOMOAB(K),HOMOSC(K),HOMOF(K)
C    PUNCH OUT THE SCATTERING KERNEL AND HOMOGENIZED CROSS SECTIONS
C    TO BE USED AS INPUT TO SPECTRUM
```

```
      WRITE(2,2000)((SIGS(I,J),I=1,30),J=1,30)
      WRITE(2,2001)(FCMOAB(K),K=1,30)
      WRITE(2,2001)(FCMOSC(K),K=1,30)
      WRITE(2,2001)(FCMOF(K),K=1,30)
      STOP
      END
      SUBROUTINE BESSEL(IC,I1,KC,K1,X)
C     THIS SUBROUTINE COMPUTES THE I AND K BESSEL FUNCTIONS IO,I1,KO, &
C     K1 FOR A GIVEN ARGUMENT X
      INTEGER R,R1
      REAL IC,I1,KC,K1,C(30)
      DATA C(1),C(2),C(3),C(4),C(5),C(6),C(7),C(8),C(9),C(10),C(11),
     1C(12),C(13),C(14),C(15),C(16),C(17),C(18),C(19),C(20),C(21),C(2
     2C(23),C(24),C(25),C(26),C(27),C(28),C(29),C(30)/255.4669,190.49
     382.48903,22.27482,4.011674,.509493, .047719,.003416,0.000192,
     4.0000C9,259.8902,181.3126,69.39592,16.33455,2.57146,.287856,
     5.023993,.001543,.000079,.000003,-21.05766, -4.56343,8.005369,
     65.283633,1.511536,.259084,.030081,.002536,.000163 ,.000008/
      T=X*X/16.-2.0
      R=-1
1     R1=R+2
      R=R+10
      D1=0
      DC=C(R+1)
2     D2=D1
      D1=DC
      DC=T*D1-D2+C(R)
      R=R-1
      IF(R.GE.R1) GO TO 2
      R=R+9
      IF(R1.NE.1) GO TO 3
      IC=(DC-D2)/2.0
      GO TO 1
3     IF(R1.NE.11) GO TO 4
      I1=X*(DC-D2)/16.0
      GO TO 1
4     KC=(DC-D2)/2.0-IC*ALOG(X/8.0)
      K1=(1.0/X-KC*I1)/IC
      RETURN
      END
```

APPENDIX D

SPECTRUM, A Code to Calculate the Flux Spectrum in the TRIGA Core

D.1 Introduction

This program was written to perform the iteration procedure described in Eqns. (28) through (34) to calculate the energy dependent flux spectrum in the core. The typical running time on the IBM 360/50 is about one minute and on the average 12 iterations are needed for the program to converge on the spectrum. The variables are defined in the FORTRAN listing and in the input data given below.

D.2 Input Data

Card 1: FORMAT(I6,2F10.4)

NG - number of groups

T - temperature in ^{o}K

Cards 2-7: FORMAT(5E15.8)

E(I) - energy of group I (eV)

Cards 8-12: FORMAT(5E15.8)

XA(I,J) - number density of element I in region J where I indicates that elements as follows: 1=H(ZrH), 2=O, 3=Al, 4=Zr, 5=U235, 6=U238, & 7=H(H_2O) and J indicates as follows: 1=fuel, 2=clad, & 3=moderator

Cards 13-14: FORMAT(5E15.8)

AA(I) - mass number of element I (as above)

Card 15: FORMAT(5E15.8)

VOL(I) - volume fraction of region I (same as J above)

Cards 58-207: FORMAT(6E13.6)

P(I,J) - macroscopic scattering kernel output from GROUPS

Cards 208-213: FORMAT(5E15.8)

SIGA(I) - homogenized absorption cross section for group I which is output from GROUPS

Cards 214-219: FORMAT(5E15.8)

SIGS(I) - homogenized scattering cross section for group I which is output from GROUPS

Cards 220-225: FORMAT(5E15.8)

SIGF(I) - homogenized fission cross section for group I which is output from GROUPS

The spectra at temperatures of 293°K and 773°K are shown in Fig. D.1.

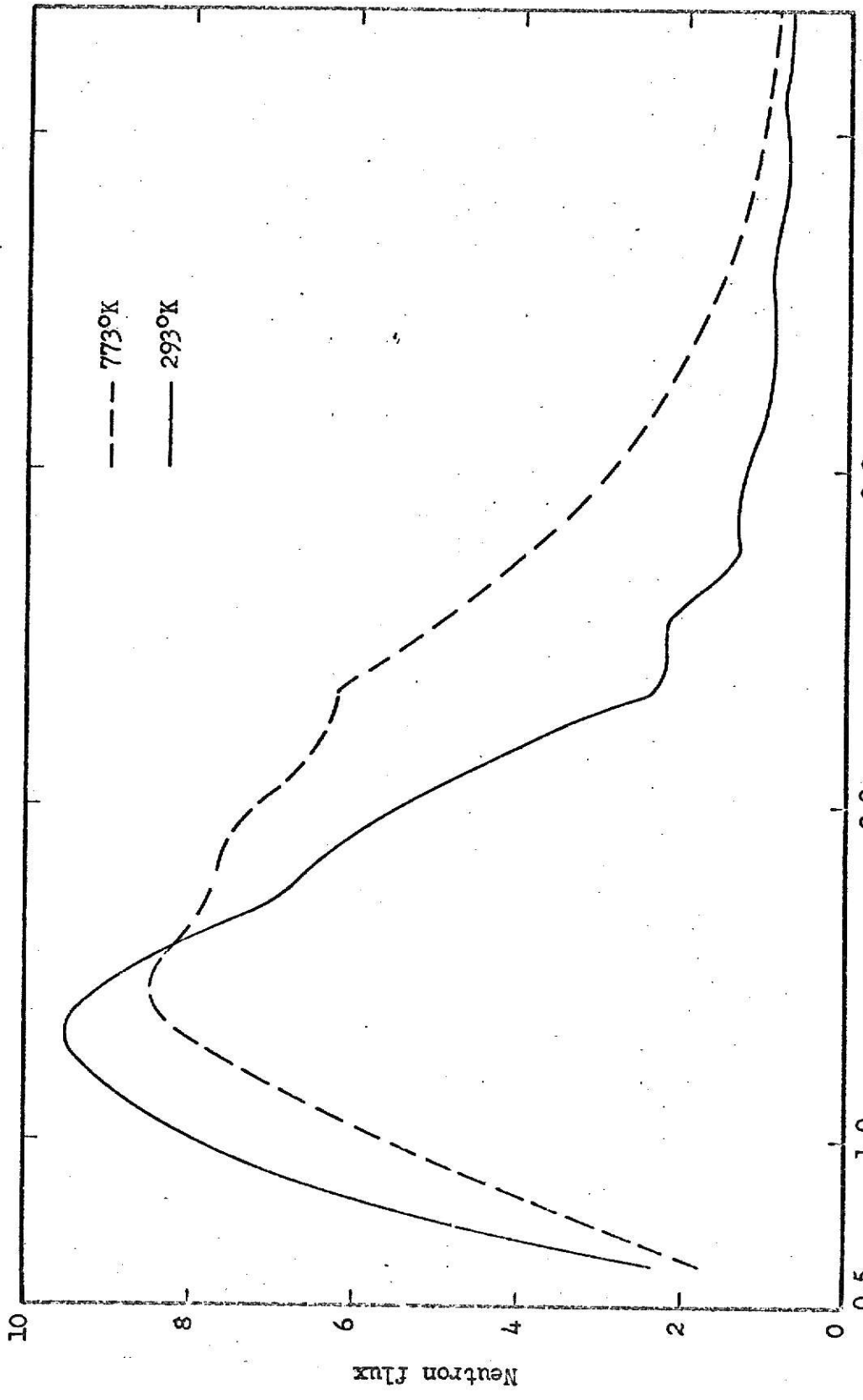

Figure D.1. Flux spectra in the TRIGA core for temperatures of 293°K and 773°K.

D.3 FORTRAN Listing of SPECTRUM

```
      COMMON/WW/ALPHA(7),VSTAR,J
      DIMENSION V(50),VM(50),P(50,50),SIGS(50),SIGA(50),SIGT(50),
     1SCB(50),XN1(50),XN2(50),XN(50),DV(50),FLUX(50),XA(7,3),
     2TABLE(3,30),AA(7),VOL(3),E(50),SIGF(50)
   12 FORMAT(I6,2F10.4)
  103 FORMAT(1H ,6X,5HGROUP,14X,7HDENSITY,18X,4HFLUX,8X,
     118HSCAT CROSS SECTION,7X,17HABS CROSS SECTION)
  104 FORMAT(1H ,5X,I4,5X,E20.8,5X,E20.8,5X,E20.8,5X,E20.8)
  105 FORMAT(///1H ,6HSIGAF=,E20.8,10X,6HSIGSF=,E20.8//5X,
     118HAVERAGE VELOCITY =,F10.4,5X,18HMEAN TEMPERATURE =,F10.4)
  107 FORMAT(1H ,20HAVG NEUTRON DENSITY=,E20.8,3X,
     117HAVG NEUTRON FLUX=,E20.8)
  109 FORMAT(1H ,12HNO OF ITER =,I6)
2000  FORMAT(6E13.6)
2001  FORMAT(5E15.8)
      EXTERNAL FCT
C   READ IN INPUT DATA
1     READ(1,12) NG,T
      IF(NG.EQ.0) CALL EXIT
      READ(1,2001)(E(I),I=1,NG)
      READ(1,2001)((XA(I,J),J=1,3),I=1,7)
      READ(1,2001)(AA(I),I=1,7)
      READ(1,2001)(VOL(I),I=1,3)
      READ(1,2001)((TABLE(I,K),K=1,NG),I=1,7)
      READ(1,2000)((P(I,J),I=1,NG),J=1,NG)
      READ(1,2001)(SIGA(I),I=1,NG)
      READ(1,2001)(SIGS(I),I=1,NG)
      READ(1,2001)(SIGF(I),I=1,NG)
C   V(I) IS THE VELOCITY AND DV(I) IS THE VELOCITY INTERVAL AROUND V(
      DO 3 I=1,NG
3     V(I)=SQRT(E(I)/0.0253)
      DV(1)=2.0*V(1)
      DV(2)=2.*(V(2)-DV(1))
      DO 9 I=3,NG
9     DV(I)=2.*(V(I)-(V(I-1)+0.5*DV(I-1)))
C   CALCULATION OF THE SOURCE SCB(I)
      DO 1000 I=1,7
1000  ALPHA(I)=((AA(I)-1.)/(AA(I)+1.))**2
      VSTAR=9.0
      DO 205 I=1,NG
      SUM=0.0
      DO 204 J=1,7
      VLOWER=ALPHA(J)*VSTAR
      DUM=0.0
      IF(V(I).LT.VLOWER) GO TO 204
      DO 230 K=1,3
      DUMDUM= XA(J,K)*TABLE(J,I)*VOL(K)*2.*V(I)*(1./(VSTAR**2)-
     1ALPHA(J)/(V(I)**2))/(1.0-ALPHA(J))
      IF(DUMDUM.GT.0.0) GO TO 230
      XL=SQRT(ALPHA(J))*VSTAR
      XL=V(I)+DV(I)/2.
      CALL QG10(XL,XL,FCT,Y)
      DUMDUM=Y*XA(J,K)*TABLE(J,I)*VOL(K)*2.
230   DUM=DUM+DUMDUM
204   SUM=SUM+DUM
205   SCB(I)=SUM
C INITIAL GUESS
      STOT=0.
```

```
      TOTAB=0.
      DO 206 I=1,NG
      XN1(I)=V(I)*V(I)*EXP(-V(I)*V(I)*293./T)
      TOTAB=XN1(I)*SIGA(I)*V(I)*DV(I) + TOTAB
  206 STOT=SCB(I)*V(I)*DV(I) + STOT
      DO 207 I=1,NG
  207 XN1(I)=XN1(I)*STOT/TOTAB
C     START ITERATION
      NIT=0
50    IF(NIT.GT.100) GO TO 3000
      B=0.
      NIT=NIT +1
      DO 208 J=1,NG
      A = 0.
      DO 209 I=1,NG
      IF(I.EQ.J) GO TO 209
      A=A +P(I,J)*XN1(I)
  209 CONTINUE
      SIGT(J)=SIGA(J) + SIGS(J)
      XN2(J) = (A+SCB(J))/(SIGT(J)-P(J,J))
      B=B+ SIGA(J)*XN2(J)*V(J)*DV(J)
  208 CONTINUE
C  RENORMALIZATION
      ITEST = 0
      DO 210 J=1,NG
      XN2(J)=XN2(J)*STOT/B
      XXX=ABS(XN2(J)-XN1(J))/XN2(J)
      IF(XXX .GT. .00001) ITEST = 1
  210 XN1(J) =XN2(J)
      IF( ITEST .EQ. 1) GO TO 50
3000  WRITE(3,109) NIT
      IF(NIT.GT.100) CALL EXIT
C    AVERAGE CROSS SECTIONS, VELOCITY, TEMPERATURE, DENSITY, AND
C    FLUX CALCULATIONS
      TERM2=0.
      SUM1X=0.0
      SUM1A = 0.
      SUM2 = 0.
      SUM1S = 0.
      SUM1F=0.0
      SUMA2=0
      SUMA3=0
      DO 212 K = 1, NG
      TERM2=TERM2 +V(K)*DV(K)
      SUM1X=SUM1X + XN1(K)*DV(K)
      TERM1 = XN1(K) * V(K) * DV(K)
      SUM1A = SUM1A + SIGA(K) * TERM1
      SUM2 = SUM2 + TERM1
      SUM1F=SUM1F+SIGF(K)*TERM1
  212 SUM1S = SUM1S + SIGS(K) * TERM1
      SIGAF = SUM1A/SUM2
      SIGSF = SUM1S/SUM2
      SIGFF=SUM1F/SUM2
      ADEN=TERM1/TERM2
      VELA=SUM2/SUM1X
      TEM=293.*(VELA/1.128)**2
      AFL=0.
      DO 220 I = 1,NG
      FLUX(I) =V(I) *XN1(I)
      AFL=AFL+FLUX(I)*V(I)*DV(I)
```

```
  220 CONTINUE
      AFLUX=AFL/TERM2
      WRITE(3,103)
      DO 213 I=1,NG
213   WRITE(3,104) I,XN1(I),FLUX(I),SIGS(I),SIGA(I)
      WRITE(3,105)SIGAF,SIGSF,VELA,TEM
      WRITE(3,107)ACEN,AFLUX
C     CALCULATION OF THE ETA-F PRODUCT FROM THE AVERAGE DATA
      XNU=2.43
      ETAFFF=XNU*SIGFF/SIGAF
      WRITE(3,215)SIGFF,SIGAF,ETAFFF
215   FORMAT('           ETA-F CALCULATION'/,'     FISSION X-SECT    A
     1RPTION X-SECT          ETA*F'/,3(5X,E14.7))
      GO TO 1
  999 CONTINUE
      STOP
      END
      SUBROUTINE QG1C(XL,XU,FCT,Y)
C     THIS SUBROUTINE  PREFORMS AN INTEGRATION OF THE EXPRESSION FOR TH
C     THE SOURCE WHEN THE ARGUMENT EVALUATED AT THE MIDPOINT IS LESS TH
C     ZERO.  THIS SUBROUTINE USES 10 POINT GAUSSIAN QUADRATURE TO EVAL-
C     UATE THE INTEGRAL.  THE INTEGRAND IS SUPPLIED BY THE FUNCTION FCT
      A=.5*(XU+XL)
      B=XU-XL
      C=.4869533*B
      Y=.0333567*(FCT(A+C)+FCT(A-C))
      C=.4325317*B
      Y=Y+.0747567*(FCT(A+C)+FCT(A-C))
      C=.3397048*B
      Y=Y+.1095432*(FCT(A+C)+FCT(A-C))
      C=.2166977*B
      Y=Y+.1346334*(FCT(A+C)+FCT(A-C))
      C=.0744371*B
      Y=B*(Y+.1477621*(FCT(A+C)+FCT(A-C)))
      RETURN
      END
      FUNCTION FCT(X)
C     THIS ROUTINE SUPPLIES THE ARGUMENT OF THE INTEGRAND AT THE VARIOU
C     GAUSS POINTS.
      COMMON/WW/ALPHA(7),VSTAR,J
      FCT=X*(1./(VSTAR**2)-ALPHA(J)/(X**2))
      RETURN
      END
```

AN ANALYSIS OF THE REACTIVITY TEMPERATURE COEFFICIENT OF THE KANSAS STATE UNIVERSITY TRIGA MARK II NUCLEAR REACTOR

by

GENE P. RATHBUN

B.S., Kansas State University, 1967

AN ABSTRACT OF A MASTER'S THESIS

submitted in partial fulfillment of the

requirements for the degree

MASTER OF SCIENCE

Department of Nuclear Engineering

KANSAS STATE UNIVERSITY
Manhattan, Kansas

1969

ABSTRACT

The TRIGA reactor has a negative temperature coefficient of reactivity which makes it very stable with respect to temperature changes in the core. The large magnitude of the negative temperature coefficient is the feature of TRIGA reactors which allows them to be pulsed to high powers. The purpose of this investigation was to determine experimentally and analytically the reactivity temperature coefficient of the Kansas State University TRIGA Mark II nuclear reactor.

The analytical investigation involved determining the temperature coefficient of the parameters which make up the effective multiplication constant. The code RABBLE was used to determine the temperature coefficient of the resonance escape probability. The temperature dependence of the ηf product was analyzed with codes developed by the author which are presented in this thesis. The temperature coefficient of the fast fission factor was assumed to be negligible. The temperature coefficient of the nonleakage probability was found by differentiating the analytical expression for the nonleakage and numerically evaluating the resulting terms.

The experimental work involved insulating a fuel element and using nuclear heat to cause reactivity pertubations due to the elevation in temperature of this element. The reactivity perturbations were recorded during both steady state and transient operation of the reactor. The data collected with the insulated element in the core were then compared with similar

data recorded when the reactor was operated with the element in the core and the insulation removed. The experimental temperature coefficient of reactivity was then determined from these two sets of data.